Thesis for the Master's degree

Electrode modification for improving the performance of bioelectrochemical cell

Advisor : Professor, Kyu-Jung Chae

Feb. 2020

Graduate School of Korea Maritime and Ocean University
Department of Civil & Environmental Engineering
Yun-Jeong Choi

Accepted in partial fulfillment of the
requirements for the Master's degree

Committee member : Prof. Young-Chae Song _____

Committee member : Prof. Kyu-Jung Chae _____

Committee member : Prof. Keun-je Yoo _____

November. 29. 2019

Graduate School of Korea Maritime and Ocean University

Table of contents

List of Tables

List of Figures

Electrode modification for improving the performance of bioelectrochemical cell

Yun-Jeong Choi

Department of Ocean Systems Engineering

Graduate School of Korea Maritime and Ocean University

Abstract

Bioelectrochemical cell (BES) is a technology that obtains energy from organic compounds by electrically active microorganisms. Depending on the form of energy, it can be divided into microbial fuel cell (MFC) that produce currents and microbial electrolysis cell (MEC) that produce high value-added materials such as methane and hydrogen. Most biochemical cells consist of anodes, cathodes, cation exchange membranes, and external power supply. Among them, electrodes are an important factor in determining MEC efficiency and focus on electrode modification to improve BES performance.

In the case of cathodes, the cost-effective electrode was fabricated to replace the high-cost Pt and applied to the MFC. Non-platinum-based metal (PGM-free) nanocatalysts were prepared using a simple and cost-effective technique called electrophoresis (EPD) and showed high catalytic oxygen reduction reaction rate (ORR) on the surface of MFC cathode. Among the catalysts without PGM, the maximum power density of 1630.7 mW m^{-2} was

obtained based on nickel nanoparticles. This value is 400% higher than the value obtained using commercial Pt catalysts under the same conditions. These results are due to the uniform deposition of Ni/NiO_x nanoparticles on the cathode, which improves electrical conductivity, catalyst activity, and long-term stability and reduces electron transfer resistance. PGM-free catalysts significantly enhanced MFC performance induced by metal/metal oxide nanoparticle layer formation and accelerated ORR.

For anodes, it was improved as a conductive polymer material to solve the inefficient problem of carbon felt (CF) commonly used and applied to MEC. CF has a high surface area with three-dimensional porosity, but since it is hydrophobic, it is not easy to move water and gas, so only electrode surfaces are used (role as a 2D electrode). To solve this problem, poly 3,4-ethylenedioxythiophene:polystyrenesulfonate (PEDOT:PSS) was used as a unique material including high conductivity (PEDOT) and hydrophilic group (PSS). PEDOT:PSS was coated on the CF surface by electropolymerization and improved durability by heat treatment at 110℃. PEDOT:PSS/CF electrode improved biocompatibility and electron transfer to the oxidation electrode by greatly improving hydrophilicity (water contact angle changed from 136.5° to 0°). As a result, the MEC using PEDOT:PSS/CF as a cathode material produced 33.4% higher hydrogen than the MEC using CF.

Overall, the performance of BES can be improved by cost-effectively modifying materials suitable for the characteristics of electrodes, which indicates significant progress in commercialization.

KEY WORDS: Electrochemical cell; Microbial fuel cell; Nickel/nickel oxide; Microbial electrolysis cell; PEDOT:PSS.

전극 개질을 통한 생물전기화학전지 효율 향상

최 윤 정

한국해양대학교 대학원

토목환경공학과

초록

생물전기화학전지(BES)는 전기화학적으로 활성을 가지는 미생물에 의해 유기화합물로부터 에너지를 얻는 기술이다. 에너지 형태에 따라 전류를 생성하는 MFC와 메탄 및 수소와 같은 고부가가치 물질을 생성하는 MEC로 나눌 수 있다. 대부분 생물전기화학전지는 산화전극, 환원전극, 양이온교환막 및 외부 전원으로 이루어져 있다. 그중에서도, 전극은 전지 효율을 결정하는 중요한 요소로, 전지 성능 향상을 위한 전극 개질에 집중한다.

환원전극의 경우, 고비용의 Pt를 대체할 수 있는 비용효과적인 전극을 제작하여 MFC에 적용하였다. 비백금계 금속(PGM-free) 나노촉매는 전기영동증착(EPD)이라는 간단하고 비용 효율적인 기술을 사용하여 제조했으며, MFC의 환원전극 표면에서 높은 촉매 산소환원반응속도(ORR)를 나타냈다. 시험된 PGM-free 촉매(Ni, Co, 및 Cd 기반) 중에서 니켈 나노 입자를 기준으로 1630.7 mW m^{-2}의 최대 전력 밀도가 달성되었다. 이 값은 동일한 조건에서 상용화된 Pt 촉매를 사용하여 얻은 값보다 400% 더 높다. 이 결과는 환원전극 상에 Ni/NiO_x 나노 입자의 얇은 층의 균일한 증착에 기인하며, 이는 전자 전달저항을 감소시키면서 전기전도도, 촉매 활성 및 장기 안정성을 개선했

다. 제조된 PGM-free 촉매는 금속/금속 산화물 나노입자 층 형태에 의해 유도된 MFC 성능 및 가속화된 ORR을 상당히 개선했다.

산화전극의 경우, MEC에 일반적으로 사용되고 적용되는 탄소펠트(CF)의 비효율적인 문제를 해결하기 위해 전도성 고분자 재료로 개선했다. CF는 3차원 다공성을 갖는 높은 표면적을 가지고 있지만 소수성이므로 물과 가스를 이동하기가 쉽지 않으므로 전극 표면만 사용된다. 이러한 문제를 해결하기 위해, poly 3,4-ethylenedioxythiophene:polystyrenesulfonate (PEDOT:PSS)를 고전도도 (PEDOT)와 친수성기 (PSS)를 포함하는 독특한 물질을 사용하였다. PEDOT:PSS는 전기중합에 의해 CF 표면에 코팅되었고 110℃에서 열처리에 의해 내구성이 향상되었다. PEDOT:PSS/CF 전극은 친수성을 크게 향상함으로써 산화전극으로의 생체적합성과 전자 전달을 개선하였다. (물 접촉각이 136.5°에서 0°로 변화됨.) 그 결과, PEDOT:PSS/CF를 산화전극으로 사용한 MEC는 CF를 사용한 MEC보다 33.4% 높은 수소를 생산하였다.

전반적으로, 전극의 특성에 맞는 재료를 사용하여 전극의 비용 효율적인 개질을 통해 BES의 성능을 향상시킬 수 있으며, 이는 BES의 상용화에 중요한 진보를 나타낸다.

KEY WORDS: 생물전기화학전지; 미생물연료전지; 니켈/니켈 산화물; 미생물전해전지; PEDOT:PSS.

Chapter 1. Literature review

1.1 Bioelectrochemical cell

Bioelectrochemical system (BES) is a sustainable technology to produce energy from organic materials in wastewater using electrically active microorganisms (exoelectrogens) which have been maximizing efficiency by donating or accepting electrons directly out of cells [1]. Therefore, it has two advantages that treat wastewater and produce energy at the same time [2]. BES is divided into cathode and anode, separated by a membrane [3]. The electron acceptor (ARB, anodic respiring bacteria) growing on the anode shares similarities in oxidizing organic matter, whereas microbial fuel cells (MFCs) and microbial electrolysis cells (MEC) depend on the type of cathode [4].

Various ARBs (Shewanella, Geobacter ext.) present in the anode oxidize organic matter in the waste stream in the anaerobic state, and electrons accumulated in the anode move to the cathode by the potential difference [5]. When the current is generated together with the oxygen reduction reaction, it is used as MEC when producing high value-added substances (hydrogen, methane, ethanol, butanol, and so on) by MFC and hydrogen reduction reaction [6]. Hydrogen is one of the main products produced by MEC as a sustainable source of green energy that does not emit greenhouse gases during combustion [7]. The basic principles of the MFC and MEC systems are shown in fig. 1.1, followed by a detailed explanation of the principles from an electrochemical aspect.
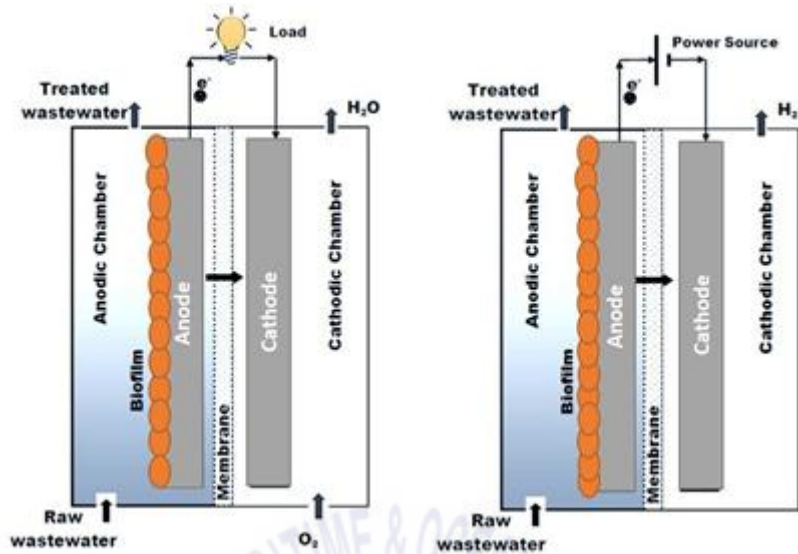
Fig. 1.1. Schematric representation of (a) electricity production from MFC and (b) hydrogen production through MEC [8].

1.1.1 Priciple of MFC and MFC in electrochemical aspects

The same reaction occurs in the MFC and MEC in the oxidation chamber (eqn. (1)). The oxidation of acetate, a substrate used mainly in neutral MFC and MEC systems, was considered. The theoretical equilibrium potential needed to oxidize 1 g L^{-1} acetate (16.9 mM) in neutral state (pH = 7) can be calculated from the Nernst equation at about -300 mV (eqn. (2)) [9].

$$CH_3COO^- + 4H_2O \rightarrow 9H^+ + 8e^- + 2HCO_3^- \quad E^{\circ} = 0.187\,V \tag{1}$$
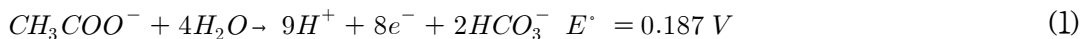
$$E_{An} = E_{An}^{\circ} - \frac{RT}{8F}ln\frac{[CH_3COO^-]}{[HCO_3^-]^2[H^+]^9}$$

$$E_{An} = 0.187 - \frac{(\frac{8.31j}{molK})(298.15K)}{8(\frac{96500C}{mol})}ln\frac{[0.0169]}{[0.005]^2[10^{-7}M]^9} = -0.300\,V$$

(2)

The Nernst potential should not depend on the anode material because the presence of the biofilm can change the kinetics of the reaction, the concentration of species in the electrolyte medium is not constant, and the calculated value of the Nernstian potential is the presence of the biofilm on the electrode surface [1, 10]. Changes in species concentration under these conditions may change the theoretical value or the reaction pathway. Thus, an additional overpotential be required.

On the other hand, the reaction is different in the cathode chamber. In MFCs, oxygen reduction reactions occur in the presence of dissolved oxygen (eqn. (3)), whereas hydrogen is produced in anaerobic conditions without dissolved oxygen in MEC (eqn. (5)). In the MFC system, the cathode Nernstian potential at the neutral state of the oxygen saturation reduction chamber and atmospheric pressure is calculated to be about 805 mV (eqn. (4)). Therefore, the balanced cell voltage of the MFC is calculated to be about 1.105 mV (= [0.805 V] − [−0.300 V]).

$$\frac{1}{2}O_2 + 2H^+ + 2e^- \to H_2O \quad E^{\circ} = 1.229\,V$$

(3)
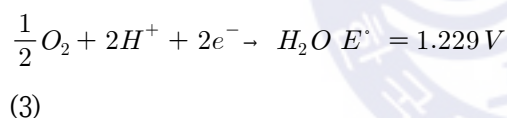
$$E_{Ca} = E_{Ca}^{\circ} - \frac{RT}{nF}ln\frac{1}{[O_2]^{1/2}[H^+]}$$

$$E_{Ca} = 1.229 - \frac{(\frac{8.31j}{molK})(298.15K)}{2(\frac{96500C}{mol})} \times \ln\frac{1}{[0.2]^{1/2}[10^{-7}M]^2} = 0.805\,V$$

(4)

The voltage calculated in the Nernst equation (eqn. (6)) at neutral (pH = 7) in the MEC system is about −0.114 V (= [−0.414 V] − [−0.300 V]). The reaction is not

spontaneous and therefore requires external energy and does not include the resistance (ohm loss, activation overpotential, and concentration, potential) within the MEC system. Therefore, hydrogen production requires a higher voltage (normal range; –0.6 to 0.5 V) than calculated [10].

$$2H^+ + 2e^- \rightarrow H_2 \ E^\circ = 0.000 \ V \tag{5}$$

$$E_{Ca} = E_{Ca}^\circ - \frac{RT}{nF} ln \frac{H_2}{[H^+]^2}$$

$$E_{Ca} = 0.0 - \frac{(\frac{8.31j}{molK})(298.15K)}{2(\frac{96500C}{mol})} \times \ln \frac{1}{[10^{-7}M]^2} = -0.414 \ V$$

(6)

Theoretically, a simple process in both reactor conditions and design, but many aspects and parameters are important when considering BES. System components in BES (e.g., electrodes, membranes, electrolytes, inoculum, and microorganism species) contribute to improving the performance of the process [11]. The role of each component in improving the bioelectrocatalyst performance of the system is then discussed.

1.2 Key configuration factors

1.2.1 Anode

The anode is a major determinant of current and biogas generation because it induces direct attachment of microbes and electron transport at the

microbial-anode interface [12]. It is important to concentrate anode-respiring bacteria (ARB) at the anode and to accelerate the rate of electron transfer [13]. This purpose can be achieved through the selection of specific electrode materials, the shape of the electrode surface and microbial culture. The electrode material and form should promote bacterial attachment and subsequent biofilm formation. At the same time, along with biofilm formation, the anode surface should enhance electron transfer from bacteria to the electrodes [14]. This requires characteristics such as high conductivity, low corrosiveness, high specific surface area and porosity, suitability for microbial growth and low cost [15].

Carbon-based materials such as carbon fiber, carbon felt, carbon paper and granular activated carbon (GAC) satisfy these properties and are widely used [16-19]. Among them, 3D porous forms of materials such as carbon brushes and carbon felts are preferred because of their large surface area [20], but the inherent hydrophobic nature of carbon-based materials limits the high performance of BES [21]. This results in insufficient adhesion of microorganisms to the electrode surface, which negatively affects microbial fixation, resulting in lower current density and increased interfacial resistance [22]. In this regard, increasing the surface area using the entire compartment of the GAC-charged anode can increase the number of ARB reactive sites. However, some reports have shown that BES performance improves when GAC is used in 3D, while other reports do not show much worse performance than similarly designed two-chambered MECs [23].

In order to solve this problem, methods of doping a conductive polymer material and a carbon-based catalyst material on a 3D porous carbon-based electrode are introduced. For example, Alae et al. used zeolites and bentonite modified CFs as anodes for MFC to increase hydrophilicity [24]. Maximum current densities were provided of 24.5 and 27.9 A m^{-2}, respectively, while an unmodified CF showed 16.9 A m^{-2} by increasing the exploitation of the

internal surface area of the 3D porous CF by electroactive biofilm. Compared to hydrophobic unmodified carbon felt, hydrophilic modified electrodes increased the utilization of the internal surface area of the 3D structure of the carbon felt by the electroactive biofilm. Mohamed et al. fabricated Fe/Fe2O3-CF (3200 mA m^{-2}), which is inexpensive and highly conductive, to reduce electron transfer resistance and showed 185% higher current density than CF (1120 mA m^{-2}) [25]. Roh et al. fabricated PPy-CNT/CF (287 mW m^{-2}) with high porosity and large surface area, resulting in a 38% improvement in power over pristine CF (208 mW m^{-2}) due to its excellent corrosion resistance, good conductivity and biocompatibility [26].

1.2.1 Cathode

Electrons and hydrogen ions generated at the anode move to the cathode and the BES type is changed according to the concentration of dissolved oxygen at the cathode. In the MFC, electrons, hydrogen, and oxygen from the anode combine to form water while saturated oxygen is dissolved in the cathode chamber [27], while MEC is advantageous for hydrogen production due to the combination of electrons and hydrogen ions under conditions of exhaustion of dissolved oxygen [28]. When there is sufficient overpotential, the cathode reaction proceeds smoothly, and the improvement of the reduction reaction rate is an important factor in determining the BES performance [29]. In addition, the voltage loss due to the ohmic resistance and interfacial electron transfer (reduced O_2 or H_2 generation) of the electrolyte at the cathode contributes significantly to the potential loss of BES [30]. Therefore, high electrical conductivity [31], large surface area [32], low cost [33], and high efficiency catalyst [34] are required as the cathode material.

In order to reduce the reaction overpotential, platinum has been used as

the most active electrocatalyst for high stability and high efficiency reduction catalysts, but expensive Pt has limited commercialization and thus requires other alternatives [35]. Carbon-based materials such as carbon paper, carbon cloth, graphite felt, and granular graphite have been mainly used to multiply microorganisms because of low cost [36-38], but they have been incompatible with platinum [39]. Recently, many studies have been reported on the development of non-platinum based cathodes comprising other transition metals [40], alloys [41], non-metal doped carbon materials [42], or reducing bacteria formatted biocathodes [43].

Zhang et al. investigated that nitrogen doped carbon nanotubes synthesized through pyrolysis bimetallic metal-organic framework Co nanoparticles nano polyhedra (AC-CoNCNT) (2252 ± 46 mW m^{-2}) showed 154% higher power density than control (AC) in air-cathode MFC [44]. Chao et al. increased MFC performance by fabricating nanorod $CoFe_2O_4$/AC (1780 ± 20 mW m^{-2}) with mesoporous structure, which has high catalyst activity and low cell resistance [45]. Kim et al. reported high hydrogen production rate and recovery ($98 \pm 5\%$.) in MEC with only a small amount of nickel by blending nickel power [46].

1.2.3 Proton exchange membrane

The PEM separates the anode chamber and the cathode chamber, and cations can be diffused through the membrane or freely exchanged with other cations for the purpose of selectively transporting only hydrogen ions [47]. In MFC, the PEM prevents oxygen diffsusion in the anaerobic anode chamber and formation biofilm in the cathode side [48]. In the MEC, the purity of hydrogen generated in the cathode is improved [49]. In addition, the PEM prevents that electron acceptor bacteria existing in the anode side infiltrate into the catholyte. On the other hand, membraneless MEC promotes the

growth of hydrogenotrophic methanogens, reducing hydrogen purity and increasing methane production efficiency.

Nafion has been the most widely used material as a PEM in BES because of its high proton conductivity, low internal resistance, and good ion exchange capacity [50]. However, Nafion is expensive to produce, accounting for approximately 40% of the total cost of MFCs [51]. To solve this problem, sulfonated hydrocarbon-based polymers, which are sulfonated porous polyether ether ketones (SPEEK) [52] and sulfonated poly (arylene ether sulfone) (SPAES) [53], glass fiber separators [54], and salt bridges [55] has been studied to replace to Nafion.

1.3 references

[1] Yasri N, Roberts EPL, Gunasekaran S. The electrochemical perspective of bioelectrocatalytic activities in microbial electrolysis and microbial fuel cells. Energy Reports. 2019;5:1116-36.

[2] Mohanakrishna G, Sandipam S, Pant D. Bioelectrochemical Systems (BES) for Microbial Electroremediation: An Advanced Wastewater Treatment Technology. 2015. p. 145.

[3] Ter Heijne A, Hamelers HV, Buisman CJ. Microbial fuel cell operation with continuous biological ferrous iron oxidation of the catholyte. Environ Sci Technol. 2007;41:4130-4.

[4] نائل يسري N. The electrochemical perspective of bioelectrocatalytic activities in microbial electrolysis and microbial fuel cells. ORNL-TM [reports] US Atomic Energy Commission. 2019;5:1116-36.

[5] Speers AM, Reguera G. Electron donors supporting growth and electroactivity of Geobacter sulfurreducens anode biofilms. Appl Environ Microbiol. 2012;78:437-44.

[6] Harnisch F, Schröder U. ChemInform Abstract: From MFC to MXC: Chemical and Biological Cathodes and Their Potential for Microbial Bioelectrochemical Systems. Chem Soc Rev. 2010;39:4433-48.

[7] Hosseini SE, Wahid M. Hydrogen Production from Renewable and Sustainable Energy Resources: Promising Green Energy Carrier for Clean Development. Renewable and Sustainable Energy Reviews. 2015;57.

[8] Roegiers I, Thijs S, Bonné R. Biochar as electron shuttle and substrate material for electroactive bacteria in a bioelectrochemical system to enhance removal of pesticides from wastewater 2018.

[9] Ajayi FF, Kim K-Y, Chae K-J, Choi M-J, Kim S-Y, Chang I-S, et al. Study of hydrogen production in light assisted microbial electrolysis cell operated

with dye sensitized solar cell. Int J Hydrogen Energy. 2009;34:9297-304.

[10] Rimboud M, Pocaznoi D, Erable B, Bergel A. Electroanalysis of microbial anodes for bioelectrochemical systems: basics, progress and perspectives. PCCP. 2014;16:16349-66.

[11] Sharma M, Alvarez-Gallego Y, Achouak W, Pant D, Sarma PM, Dominguez-Benetton X. Electrode material properties for designing effective microbial electrosynthesis systems. Journal of Materials Chemistry A. 2019;7:24420-36.

[12] Malvankar N, Lovley D. Microbial Nanowires: A New Paradigm for Biological Electron Transfer and Bioelectronics. ChemSusChem. 2012;5:1039-46.

[13] Sasaki D, Sasaki K, Tsuge Y, Kondo A. Less biomass and intracellular glutamate in anodic biofilms lead to efficient electricity generation by microbial fuel cells. Biotechnology for Biofuels. 2019;12:72.

[14] Santoro C, Babanova S, Artyushkova K, Cornejo J, Ista L, Marsili E, et al. Influence of Anodes Surface Chemistry on Microbial Fuel Cells Operation. Bioelectrochemistry. 2015;106.

[15] Wei J, Liang P, Huang X. Recent progress in electrodes for microbial fuel cells. Bioresour Technol. 2011;102:9335-44.

[16] Tursun H, Liu R, Li J, Abro R, Wang X, Gao Y, et al. Carbon Material Optimized Biocathode for Improving Microbial Fuel Cell Performance. Frontiers in Microbiology. 2016;7.

[17] Liang P, Wang H, Xia X, Huang X, Mo Y, Cao X, et al. Carbon nanotube powders as electrode modifier to enhance the activity of anodic biofilm in microbial fuel cells. Biosens Bioelectron. 2011;26:3000-4.

[18] Yang Q, Zhao X, Yang J, Zhou B, Wang J, Dong Y, et al. Welding assembly of 3D interconnected carbon nanotubes on carbon fiber as the high-performance anode of microbial fuel cells. Int J Hydrogen Energy. 2019;44:20304-11.

[19] Tursun H, Liu R, Li J, Abro R, Wang X, Gao Y, et al. Carbon material

optimized biocathode for improving microbial fuel cell performance. Frontiers in microbiology. 2016;7:6.

[20] Wang X, Cheng S, Feng Y, Merrill MD, Saito T, Logan BE. Use of carbon mesh anodes and the effect of different pretreatment methods on power production in microbial fuel cells. Environ Sci Technol. 2009;43:6870-4.

[21] Santoro C, Guilizzoni M, Baena JC, Pasaogullari U, Casalegno A, Li B, et al. The effects of carbon electrode surface properties on bacteria attachment and start up time of microbial fuel cells. Carbon. 2014;67:128-39.

[22] Borole AP, Reguera G, Ringeisen B, Wang Z-W, Feng Y, Kim BH. Electroactive biofilms: current status and future research needs. Energy Environ Sci. 2011;4:4813-34.

[23] Yasri NG, Nakhla G. The performance of 3-D graphite doped anodes in microbial electrolysis cells. J Power Sources. 2017;342:579-88.

[24] Elabed A, El Khalfaouy R, Saad I, Basseguy R, El Abed S, Erable B. Low-Cost Electrode Modification to Upgrade the Bioelectrocatalytic Oxidation of Tannery Wastewater Using Acclimated Activated Sludge. Applied Sciences. 2019;9:2259.

[25] Mohamed HO, Obaid M, Poo K-M, Ali Abdelkareem M, Talas SA, Fadali OA, et al. Fe/Fe2O3 nanoparticles as anode catalyst for exclusive power generation and degradation of organic compounds using microbial fuel cell. Chem Eng J. 2018;349:800-7.

[26] Roh S-H, Woo H-G. Carbon nanotube composite electrode coated with polypyrrole for microbial fuel cell application. Journal of nanoscience and nanotechnology. 2015;15:484-7.

[27] Halim M. Effect of Various Operating Parameters on Power Generation from Mediator Less Microbial Fuel Cell: Khulna University of Engineering & Technology (KUET), Khulna, Bangladesh; 2019.

[28] Zhang L, Wang Y-Z, Zhao T, Xu T. Hydrogen production from simultaneous saccharification and fermentation of lignocellulosic materials in a

dual-chamber microbial electrolysis cell. Int J Hydrogen Energy. 2019;44:30024-30.

[29] Cho S-K, Lee M-E, Lee W, Ahn Y. Improved hydrogen recovery in microbial electrolysis cells using intermittent energy input. Int J Hydrogen Energy. 2019;44:2253-7.

[30] Hua T, Li S, Li F, Zhou Q, Ondon BS. Microbial electrolysis cell as an emerging versatile technology: a review on its potential application, advance and challenge. Journal of Chemical Technology & Biotechnology. 2019;94:1697-711.

[31] Hu J, Zeng C, Liu G, Lu Y, Zhang R, Luo H. Enhanced sulfate reduction accompanied with electrically-conductive pili production in graphene oxide modified biocathodes. Bioresour Technol. 2019;282:425-32.

[32] Yuan Y, Zhang J, Xing L. Effective electrochemical decolorization of azo dye on titanium suboxide cathode in bioelectrochemical system. International Journal of Environmental Science and Technology. 2019:1-12.

[33] Liu W, Wang L, Gao L, Wang A-J. Hydrogen and Methane Production in Bioelectrochemical System:: Biocathode Structure and Material Upgrading. Microbial Electrochemical Technology: Elsevier; 2019. p. 921-53.

[34] Majidi MR, Farahani FS, Hosseini M, Ahadzadeh I. Low-cost nanowired α-MnO2/C as an ORR catalyst in air-cathode microbial fuel cell. Bioelectrochemistry. 2019;125:38-45.

[35] Shahane S, Choudhury P, Tiwari O, Mishra U, Bhunia B. Exoelectrogenic Bacteria: A Candidate for Sustainable Bio-electricity Generation in Microbial Fuel Cells. Waste to Sustainable Energy: MFCs-Prospects through Prognosis. 2019.

[36] Koo B, Lee S-M, Oh S-E, Kim EJ, Hwang Y, Seo D, et al. Addition of reduced graphene oxide to an activated-carbon cathode increases electrical power generation of a microbial fuel cell by enhancing cathodic performance. Electrochim Acta. 2019;297:613-22.

[37] Choudhury P, Prasad Uday US, Bandyopadhyay TK, Ray RN, Bhunia B. Performance improvement of microbial fuel cell (MFC) using suitable electrode and Bioengineered organisms: A review. Bioengineered. 2017;8:471-87.

[38] Tursun H, Liu R, Li J, Abro R, Wang X, Gao Y, et al. Carbon Material Optimized Biocathode for Improving Microbial Fuel Cell Performance. Frontiers in microbiology. 2016;7:6-.

[39] Sawant SY, Han TH, Cho MH. Metal-Free Carbon-Based Materials: Promising Electrocatalysts for Oxygen Reduction Reaction in Microbial Fuel Cells. Int J Mol Sci. 2016;18:25.

[40] Kang S, Kim H, Chung Y-H. Recent developments of nano-structured materials as the catalysts for oxygen reduction reaction. Nano Converg. 2018;5:13-.

[41] Włodarczyk PP, Włodarczyk B. Wastewater treatment and electricity production in a microbial fuel cell with Cu-B alloy as the cathode catalyst. Catalysts. 2019;9:572.

[42] Lv K, Zhang H, Chen S. Nitrogen and phosphorus co-doped carbon modified activated carbon as an efficient oxygen reduction catalyst for microbial fuel cells. RSC Advances. 2018;8:848-55.

[43] Prakasam V, Bagh F, Ray D, Fifield B-A, Porter L, Lalman J. Role of Biocathodes in Bioelectrochemical Systems. 2018. p. 165-87.

[44] Zhang S, Su W, Wang X, Li K, Li Y. Bimetallic metal-organic frameworks derived cobalt nanoparticles embedded in nitrogen-doped carbon nanotube nanopolyhedra as advanced electrocatalyst for high-performance of activated carbon air-cathode microbial fuel cell. Biosens Bioelectron. 2019;127:181-7.

[45] Ren C, Li K, Lv C, Zhao Y, Wang J, Guo S. Nanorod CoFe2O4 modified activated carbon as an efficient electrocatalyst to improve the performance of air cathode microbial fuel cell. J Electroanal Chem. 2019;840:134-43.

[46] Kim K-Y, Logan BE. Nickel powder blended activated carbon cathodes for hydrogen production in microbial electrolysis cells. Int J Hydrogen Energy.

2019;44:13169-74.

[47] Chae K-J, Kim K-Y, Choi M-J, Yang E, Kim IS, Ren X, et al. Sulfonated polyether ether ketone (SPEEK)-based composite proton exchange membrane reinforced with nanofibers for microbial electrolysis cells. Chem Eng J. 2014;254:393-8.

[48] Liu H, Logan BE. Electricity generation using an air-cathode single chamber microbial fuel cell (MFC) in the absence of a proton exchange membrane. ACS, Division of Environmental Chemistry-Preprints of Extended Abstracts2004. p. 1485-8.

[49] Planell NM. Hydrogen production from wastewater in single chamber microbial electrolysis cells: studies towards its scaling-up: Universitat Autònoma de Barcelona; 2014.

[50] Flimban SG, Hassan SH, Rahman MM, Oh S-E. The effect of Nafion membrane fouling on the power generation of a microbial fuel cell. Int J Hydrogen Energy. 2018.

[51] Hernández-Flores G, Solorza-Feria O. Comparison of alternative membranes to replace high cost Nafion ones in microbial fuel cells. Int J Hydrogen Energy. 2016.

[52] Gahlot S, Kulshrestha V. Dramatic improvement in water retention and proton conductivity in electrically aligned functionalized CNT/SPEEK nanohybrid PEM. ACS applied materials & interfaces. 2014;7:264-72.

[53] Park S-G, Chae K-J, Lee M. A sulfonated poly(arylene ether sulfone)/polyimide nanofiber composite proton exchange membrane for microbial electrolysis cell application under the coexistence of diverse competitive cations and protons. J Membr Sci. 2017;540.

[54] Li W-W, Sheng G-P, Liu X-W, Yu H-Q. Recent advances in the separators for microbial fuel cells. Bioresour Technol. 2010;102:244-52.

[55] Min B, Cheng S, Logan B. Electricity Generation Using Membrane and Salt Bridge Microbial Fuel Cells. Water Res. 2005;39:1675-86.

Chapter 2.

Electrophoretically fabricated nickel/nickel oxides as cost effective nanocatalysts for the oxygen reduction reaction in air-cathode microbial fuel cell

2.1 Introduction

Global energy scarcity and the continuous production of wastewater effluent are considered the most serious challenges facing the world and hinder socio-economic development. In recent times, microbial fuel cell (MFC) technology has attracted significant attention due to advantages such as high conversion efficiency and environmental friendliness [1]. Interestingly, this technique allows the simultaneous production of energy and degradation of organic pollutants in wastewater [2, 3]. An air-cathode MFC typically consists of anodic and cathodic chambers separated by a proton exchange membrane. In the anodic chamber, exoelectrogenic microorganisms oxidize organic substrates via metabolic reactions, generating electrons and protons that are moved to the cathode chamber by the external circuit and proton exchange membrane, respectively [4]. On the cathode surface and under aerobic conditions, the electrons reduce oxygen, which combines with protons, producing a non-toxic reduction product (i.e., water) [5]. Despite the advantages of MFCs, their large-scale application is restricted by the low

catalytic activity of the oxygen reduction reaction (ORR) [6], low production of power [7], and the high cost of their components [8]. Therefore, significant efforts have been devoted to the enhancement of MFC performance by optimizing a variety of operational factors such as electrode type [9], catalyst material [10], wastewater conditions [11], bacterial cultures [12], and substrate concentration.

Among these parameters, the catalyst material plays a critical role in improving the performance of MFCs due to its direct effect on the ORR, which is considered the main parameter limiting the generated power of MFCs. Moreover, the ORR catalyst materials represent more than 50% of the total cost of MFCs [13]. It has been known for several years that Pt is an efficient ORR catalyst for MFCs, due to the rapid kinetics of the oxidation reduction reaction and its high catalytic activity. Nevertheless, its high cost, limited availability, poor durability, and tendency to cause surface poisoning (especially when using wastewater) have restricted the widespread or large-scale application of MFCs using a Pt-based catalyst [14, 15]. Such concerns have prompted researchers to develop alternative non-precious catalyst materials with high ORR electrocatalytic activity for use in MFC scale-up. In general, catalyst materials can be classified as biotic or abiotic. Biotic catalyst materials, such as enzymes or bacteria, are extremely active and more selective in neutral media, but their high cost and poor durability restrict their application in MFCs [16]. Moreover, the electron transfer mechanisms for these biomaterials are not fully understood, especially in wastewater media [17]. Abiotic catalysts are mainly subdivided into three groups: carbonaceous materials [18], Pt group metal (PGM) catalysts [19], and PGM-free catalysts [20]. With their high chemical resistances, good stabilities, long lifetimes, and cost efficiencies, PGM-free catalysts (i.e., Fe, Mn, Co, Cd, and Ni) are superior to PGM catalysts, and have higher or comparable

electrochemical performance [21, 22]. In this context, many researchers have investigated carbon-supported PGM-free catalysts electrodes, such as MnO_2-graphene hybrids [23] and manganese oxide (MnOx) supported on a nitrogen-doped carbonaceous electrode, [14] as cathode materials for MFCs. Interestingly, the results of such investigations have shown comparable electrochemical performance with those achieved with a Pt catalyst electrode. Furthermore, carbon-nanotube-doped transition metals such as Fe and Co have exhibited higher electrocatalytic activity and good stability with respect to ORR compared to a commercial Pt/C electrode [24]. In addition, a carbon-supported Ni composite electrode has shown excellent potential for use as an alternative cathode material in MFCs [25]. However, most of these previous studies demonstrated that the fabrication technique has a significant effect on the catalytic activity of the PGM-free catalyst electrode [23].

Consequently, several techniques have been investigated in previous studies, such as chemical vapor deposition [26], hydrothermal treatment [27], brushing [28], and sol-gel techniques [29]. However, most of these investigated techniques are expensive, complicated, time-consuming, and require specific conditions such as high temperature and pressure. In addition, the generated power and current densities of MFCs based on those techniques is insufficient for large-scale applications. Therefore, developing an efficient and appropriate strategy for fabricating an alternative, non-precious catalyst with high conductivity and large exposed active sites (while maintaining effective stability) is necessary for achieving optimal performance of MFCs.

In this study, EPD is introduced as a simple, cost-effective, and scalable technique to prepare Ni, Cd, and Co nanoparticle catalyst layers on a carbon-felt (CF) cathode material for use as efficient PGM-free catalytic cathode materials for single-chamber air-cathode MFCs. The performance of the fabricated PGM-free catalyst cathodes has been investigated and

Collection @ kmou

compared to that of the Pt-coated carbon cathode in a single air-cathode MFC. This study compares the performances of MFCs employing three different PGM-free nanocatalysts. In addition, it introduces detailed procedures for a simple and cost-effective fabrication technique, along with an in-depth discussion about the unique features based on morphology, chemical composition, catalytic activity, and electrical resistivity of the prepared catalyst materials. These considerations have not been well-described in previous studies. Overall, this study introduces a new approach for the improvement of MFC application on a large scale, based on economic viability of PGM-free cathode catalyst materials.

2.2. Materials and methods

2.2.1. Electrode fabrication

A CF (3 × 3 cm, 2.5 mm thickness, purchased from Morgan, UK) was used as the cathode base material for MFCs. First, CF was cleaned by sonication in acetone for 12 hours to remove impurities and then immersed in deionized water for 20 h and dried overnight in a drying oven at 70℃. The PGM-free catalyst layers were fabricated on the surface of CF cathodes using EPD, as described in a previous study [30]. To electrophoretically fabricate a cathode, two carbonaceous electrodes were immersed in an electrolytic cell containing 500 mL of a target metal precursor solution (190 mM), depending on the selected catalyst materials (Ni, Co, and Cd). The catalyst precursors were $NiCl_2 \cdot 6H_2O$, $CdCl_2 \cdot 6H_2O$, and $CoCl_2 \cdot 6H_2O$, which were purchased from Samchun chemicals (South Korea). An external power supply was used to adjust the difference of voltage between the two electrodes at 30 V for 30 min. As a result, CF cathodes covered with PGM-free catalyst layers were obtained. The prepared cathodes are denoted as Ni/CF, Cd/CF, and Co/CF for

- 18 -

the nickel, cadmium, and cobalt-doped CF, respectively. A commercial Pt-coated carbon-based cathode (purchased from Chem Inc., USA) was utilized as a control cathode (denoted as Pt/C).

2.2.2. MFC assembly and operation

The utilized reactors of MFC reactors have identical dimensions of 5 × 2.5 × 8 cm, with a total volume of 100 mL (84 mL working volume + 20 mL head space). MFCs were operated under batch mode at room temperature. The anode material was commercial CF and the cathode material was CF coated with PGM-free catalyst layers. One side of the coated cathode faced the cation exchange membrane (CEM, CMI-7000), which was purchased from Membrane International Inc. (USA). The other side was directly exposed to air (i.e., an air-cathode configuration). The distance between two electrodes was fixed at 3.5 cm.

The MFC was inoculated with anaerobic sludge collected from the Sooyoung wastewater treatment plant in Busan (South Korea) under oxygen-free conditions. The anaerobic digester sludge had the following characteristics: total suspended solids (TSS) 11525 mg L^{-1}, volatile suspended solids (VSS) 4147 mg L^{-1}, chemical oxygen demand (COD) 5849 mg L^{-1}, pH 8.23, and electrical conductivity (EC) 6.84 mS cm^{-1}. To support bacterial growth, the wastewater sludge was diluted in a 1:3 ratio with an autoclaved anaerobic nutrient buffer solution, as described in a previous study [29]. The diluted anaerobic sludge was then purged using nitrogen gas for 20 min to remove the remaining oxygen before and after inoculation into the MFC. As a carbon source, acetic acid was injected into the MFC at an 80 mM concentration. In order to analyze the bacterial and archaeal communities, the microflora in anaerobic sludge was examined by next generation-sequencing

(Ion PGM™ System, Life Technologies, USA).

2.2.3. Material characterizations

The crystal structures of the prepared PGM-free catalyst cathode materials were investigated using an x-ray advanced diffractometer system (XRD, RIGAKU, Japan). Diffraction patterns were recorded over 2θ from $10°$ to $90°$ at a step rate of $0.05°$. The morphology of the prepared cathodes was investigated with a field-emission scanning electron microscope (FE-SEM, Tescan, Czech Republic), which was equipped with an energy dispersive X-ray (EDX) analysis tool. TEM images were observed using high-resolution transmission electron microscopy (HR-TEM, JEOL, Japan). The element compositions of the prepared cathode were analyzed using Fourier-transform infrared spectroscopy (FT-IR, Spectrum GX, Perkin Elmer, USA) in the range of $650–4000$ cm^{-1} and Raman spectroscopy (DXR, Thermo Scientific, USA) with laser excitation at 532 nm.

2.2.4. Electrochemical measurements and polarization curves

Open circuit voltage (OCV) and electrode potentials were measured versus time using a multimeter (Model 2700, KEITHLEY, USA) and Ag/AgCl reference electrodes (RE-1B; AS, Japan), respectively. After stabilization of the OCV, the cell circuit was closed, and polarization curves were then attained under various external resistances (10 to 1300 kΩ). Currents were calculated using Ohm's law, as shown in Eq. (1).

$I = V/R$ (1)

Here, I (A) is current, V (V) is voltage, and R (Ω) is applied external resistance. The electrocatalytic activity of the prepared cathode materials was

investigated using cyclic potentiostatic voltammetry (CV, ZIVE SP1, WonATech, Korea) in a three-electrode cell. In which, the fabricated PGM-free catalyst electrode was connected as the working electrode, whereas Ag/AgCl and a Pt wire were used as the reference and counter electrodes, respectively.

The actual conversion efficiency of the MFCs was measured using the coulombic efficiency (CE) equation, which represents the ratio of the actual generated current to the theoretical current that should be generated as a result of organic substrate degradation by microorganisms in the MFC. The CE of batch mode MFCs can be calculated as described in a previous study using Eq. (2) [31].

$$CE = \frac{M \int_0^t I dt}{F b V_{an} \triangle COD} \tag{2}$$

The overall internal resistance of the MFC based on pristine and fabricated PGM-free catalyst cathodes was calculated using the slope of the polarization curve ($\triangle E/\triangle I$). Finally, the current stability was investigated for two days at a constant voltage of 0.2 V. Moreover, the COD before and after MFC experiments was measured using an HS COD-LR kit (Humas, HS 2300 plus, Korea).

2.3. Results and discussion

2.3.1. Morphology of the fabricated cathodes

Fig. 2.1 shows the FE-SEM and HR-TEM characterization of pristine and fabricated PGM-free catalyst cathodes materials. As shown in the FE-SEM images, the pristine CF fibers were smoothly interlinked (Fig. 2.1a), unlike the coated CF fibers (Figs. 2.1b, c, and d), which are evenly covered with metal nanoparticles, exhibiting an intertwined network porous microstructure morphology. This porous structure is attributed to the spreading growth of prickly catalyst nanoparticles with numerous bumps on the surface of the CF cathode. Notably, the morphologies of the synthesized nanoparticle coating layers were different from one metal to another. These results are attributed to the significant difference in metal morphology, chemical structure, crystallinity, wettability, and roughness of the surface from one metal layer to another (Figs. 2.1b, c, and d).

Furthermore, the HR-TEM images of Ni nanoparticles show a uniform distribution and lack of agglomeration (Fig. 2.1e) on the surface of CF, in comparison with Cd- and Co-distributed nanoparticles (Figs. 2.1f and g). The uniform distribution of Ni nanoparticles increases the surface area as well as enhances the active sites on the cathode surface. This, in turn, led to an improvement in mass transfer diffusion and accelerated the rate of ORR [28], while also enhancing the electron pathway toward water generation on the cathode surface (instead of producing hydrogen peroxide as an unfavorable intermediate by-product) [32].
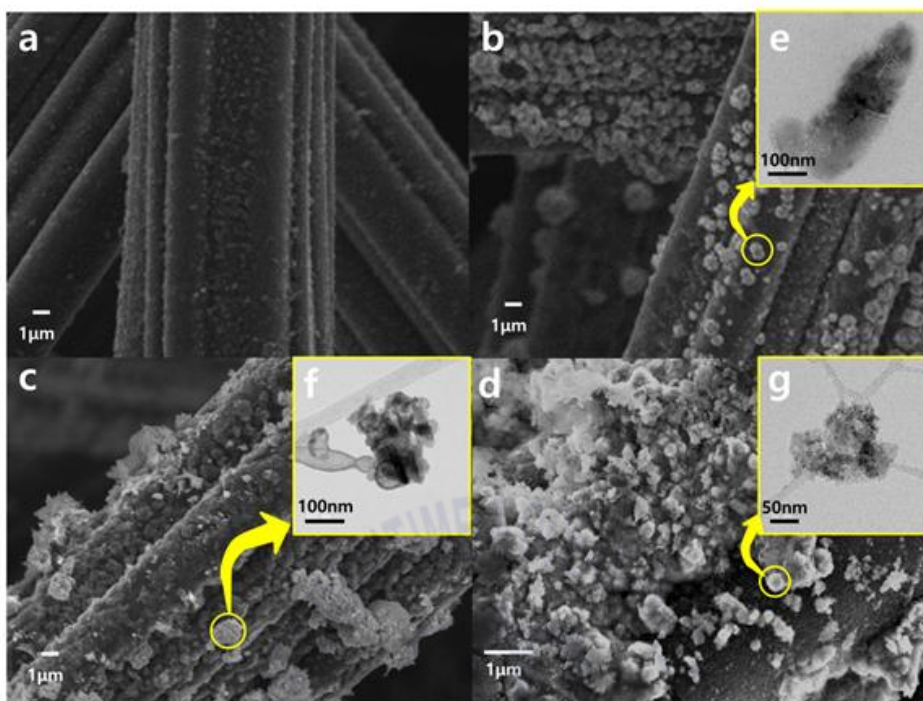
Fig. 2.1. FE-SEM and HR-TEM images (inset) of (a) CF, (b and e) Ni/CF, (c and f) Cd/CF, and (d and g) Co/CF cathodes.

2.3.2. Chemical structure of the fabricated cathodes

EDX mapping was conducted to confirm the chemical composition of the synthesized PGM-free catalytic cathode materials. As shown in Fig. 2.2, Ni, Cd, and Co were clearly detected on the surface of PGM-free catalyst cathode materials that were investigated. Remarkably, carbon exhibited the lowest percentage for the PGM-free catalyst fabricated cathodes, implying that most of the surface area of the investigated cathodes was covered by a metal or metal-oxide layers. These results are in accordance with the obtained FE-SEM results (Fig. 2.1). Moreover, as shown by the EDX mapping in Fig. 2.2a, the Ni/CF cathode has the highest oxygen content, indicating that

the created nickel nanoparticles on the surface of the CF electrode material were in the form of nickel-sheathed nickel-oxide nanoparticles, which was also confirmed by XRD analysis (Fig. 2.3a).
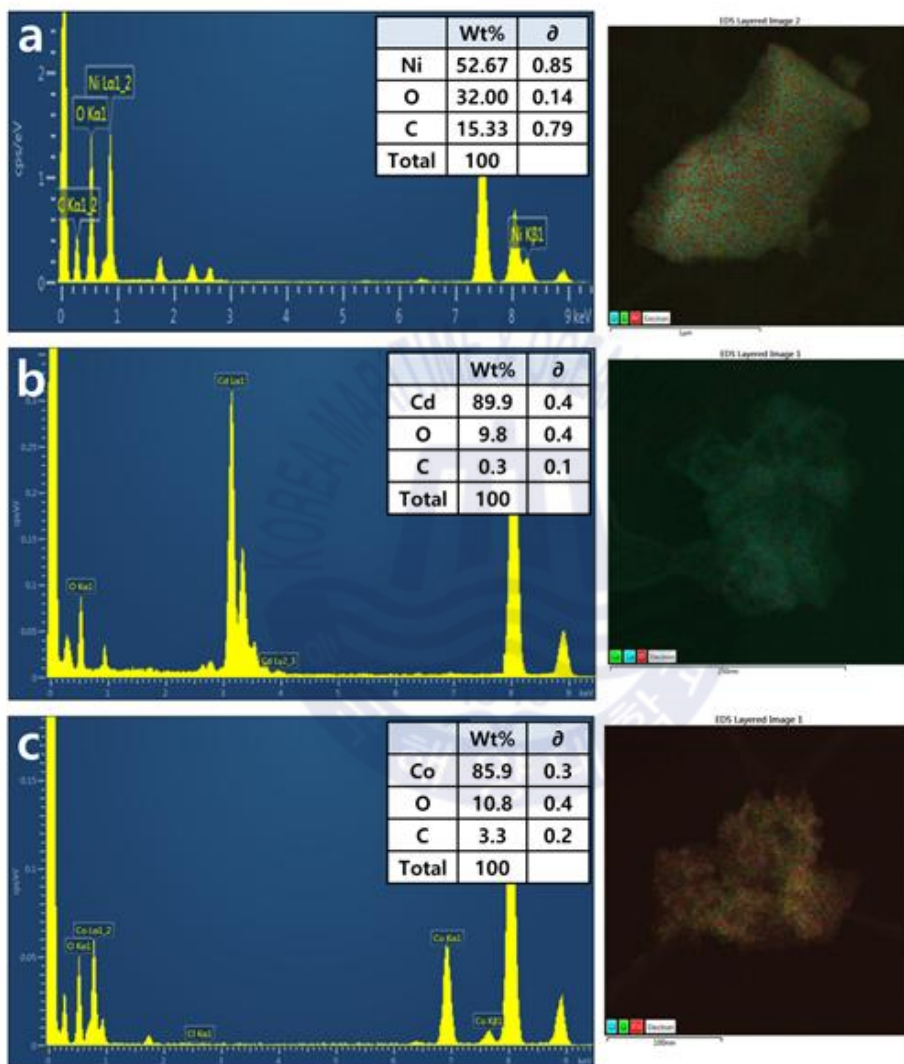
Fig. 2.2. EDX spectra of the fabricated (a) Ni/CF, (b) Cd/CF, and (c) Co/CF cathodes.

The crystal structures of the fabricated PGM-free cathodes were investigated using XRD analysis, as shown in Fig. 2.3a. As shown by Fig. 2.3a, a broad peak appeared at 23° for all investigated cathode materials, which is attributed to carbon material corresponding to the (003) structure plane based on the JCPDS database (No. 15-0806). Moreover, for the Ni/CF cathode, the observed peaks at 2θ values of 47.66° and 58° confirm the formation of nickel nanoparticles on the CF surface, which were assigned to the (111) and (200) Ni crystal planes, respectively [32]. The remaining diffraction peaks at 34°, 38.33°, 42.82°, and 61° are attributed to (003), (111), (200), and (220) NiO_x planes [33]. For Cd/CF, the observed peaks at 2θ of 34.4°, 39.4° and 56.2° correspond to (002), (101), and (102) cadmium crystal planes, respectively [34]. The pattern of Co/CF contains three reflections from the Co (111), (200), and (220) planes at 43.28°, 54.2°, and 78.6°, respectively [35, 36]. These results indicate the successful deposition of Co and Cd nanoparticle metallic layers on the surface of the CF cathode materials. In contrast, Ni/CF cathode material exhibited Ni sheathed by a NiO_x nanoparticle layer under the same conditions of the fabrication process. The formation of a Ni/NiO_x catalyst layer is mainly attributed to the high metallic activity of Ni compared to Cd and Co metals, which led to oxidized Ni in the presence of oxygen. These results were also confirmed by the Raman spectra in the range of 3500–500 cm^{-1} (as shown in Fig. 2.3b).

Fig. 2.3b shows the Raman spectra for all investigated cathode materials. As shown by Fig. 2.3b, the Raman spectra show two prominent peaks for all investigated cathodes. This can be attributed to the D band peak (structure defects and disorders) that are commonly located at 1358 cm^{-1} and the G band peak (graphitization), which is observed at approximately 1589 cm^{-1}. The deposition of transition metals (Ni, Co, and Cd) affected the D and G bands, while the Raman bands intensities (ID/IG) were decreased from 1.60 for CF

pristine cathode to be, 1.25, 1.14, and 1.03, for Ni/CF, Cd/CF and Co/CF, respectively. This changing of (ID/IG) value, is attributed to the change in purity, geometry, structure, crystallinity, and surface composition of the CF base electrode following the EPD process. However, it can be observed from Fig. 2.3b that Ni/CF exhibited a new peak at around 508 cm^{-1}, which was attributed to the NiO_x, while no new peaks were observed for Cd/CF and Co/CF, where the metals are Raman silent [37]. These results confirmed the deposition of Cd, Co, and Ni/NiO_x on the surface of CF cathodes. In other words, the ID/IG ratio is important in evaluating structural changes on the surface of the CF pristine electrode due to the EPD coating process.

Fig. 2.3c shows the surface chemical structure of the CF, Ni/CF, Cd/CF, and Co/CF materials obtained by FT–IR analysis. As shown in Fig. 2.3c for CF, graphite (carbon) stretching vibrations were observed at 3900 cm^{-1}, and the weak peaks at 2928, 2844, and 2354 cm^{-1} are attributed to OH bending and OH (free) asymmetric stretching of water. These can be attributed to the water (humidity) absorbed from the surrounding atmosphere. Furthermore, the weak peaks observed between 1600 and 1400 cm^{-1} are related to carbon. For Ni/CF, a band related to $Ni(OH)_2$ was found at 3640 cm^{-1}, and the intense peak at 678 cm^{-1} was attributed to a Ni-O stretching band. Moreover, strong peaks at 3354 cm^{-1} (OH-free asymmetric stretching), 2928 cm^{-1} (OH bending), 2844 cm^{-1} (OH bending), 1738 cm^{-1} (C=O stretching), 1610 cm^{-1} (H-O-H bending), and 1058 cm^{-1} (C-O stretching) appeared in the spectra of all the fabricated cathodes [38]. These peaks may be due to hydrolysis, because the voltage used in EPD is greater than the ideal theoretical voltage for hydrolysis (1.23 V). In summary, the FT-IR results are consistent with the XRD analysis.
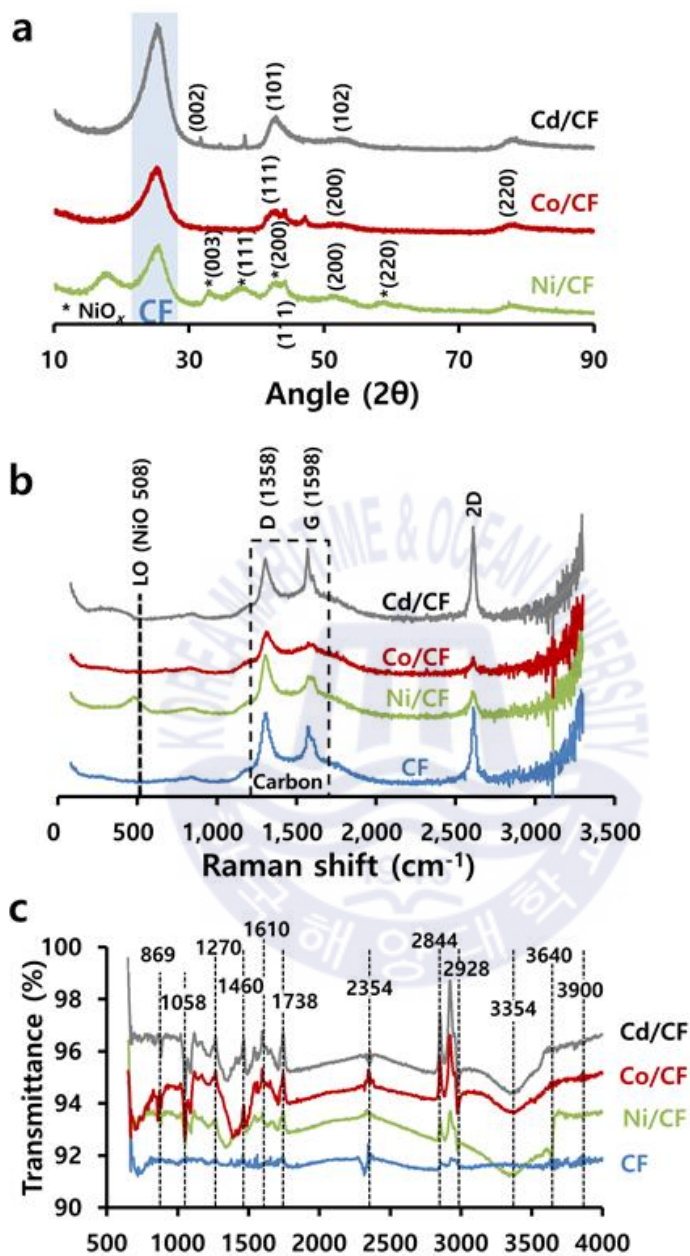
Fig. 2.3. (a) X-ray photoelectron spectra, (b) Raman spectra, and (c) FT-IR spectra of pristine and the PGM-free catalyst cathodes.

2.3.3. Oxygen reduction reaction characteristics

In order to investigate the catalytic activity of the fabricated cathode catalyst materials, CV measurements were conducted in 20 mL of the wastewater solution at room temperature before and after the metal electrodeposition process. As shown in the CV curves, Fig. 2.4a, there are no obvious peaks for the pristine CF electrode, indicating that no electrochemical reactions occurred at the selected potential and scan rate [28]. However, three different reduction peaks were observed for Ni/CF, Cd/CF, and Co/CF, suggesting that the catalytic activity of CF as a cathode material is mainly attributed to the deposition of Ni, Cd, and Co nanoparticles on the surface of the CF base electrode.

Moreover, the Ni-sheathed NiO_x nano-catalyst material exhibited the highest peak in current density compared to the other fabricated catalyst materials. This means that Ni/CF has the highest catalytic activity with respect to the ORR compared to the other cathode catalyst materials. Although, Ni/CF and Pt/C exhibited maximum reduction peaks at the same potential, the Ni/CF cathode achieved a higher current density compared to the Pt/C cathode. This is probably due to the high electrical conductivity of the nickel nanoparticles coupled with the high affinity of NiO_x for oxygen chemisorption during ORR, which prevents hydrogen peroxide (H_2O_2) generation on the surface of the cathode catalyst material [39]. In addition, under oxygen-saturated conditions, the current density of the reduction peaks for the Ni/CF catalyst was increased (Fig. 2.4b) compared to that achieved under oxygen-free conditions (Fig. 2.4a). The achieved current density at the cathodic onset potential for Ni/CF were 10 mA cm^{-2} and 15 mA cm^{-2} for oxygen-free and under saturated oxygen solution respectively. This increase in the cathodic current density is due to the high affinity and capability of the Ni-sheathed NiO_x nanoparticles for the ORR under oxygen conditions [40]. It is worth to mention that, the

obtained value of cathodic current density based on Ni/CF is 15-times higher than that (1.08 mA cm^{-2}) achieved in other studies [41] in which Ni-coated carbon-based electrodes were synthesized using a chemical reduction modification technique. The significant increase in current produced in this study would be attributed to the uniform distribution of Ni/NiO$_x$ nanoparticles on the CF electrode, which resulted in a higher surface area, a larger number of active sites and excellent wettability, which in turn led to a decrease in electron transfer resistance and enhancement of the mass transfer rate. This facilitated the ORR kinetics reaction on the cathode surface, resulting in an increase in the produced current and power densities.

In general, the ORR on the cathode surface occurs via two pathways: a two-electron pathway involving the formation of H$_2$O$_2$ ions as an intermediate product, or a four-electron pathway that produces water as the end product of the combination of hydrogen and oxygen. H$_2$O$_2$ ions are corrosive and can be the cause of many problems, such as, membrane damage or electrode corrosion. Therefore, the four-electron pathway is more favorable than the two-electron pathway [42].

The schematic pathways for the ORR on the surface of the Ni-sheathed NiO$_x$ nanoparticle catalyst materials. The ORR on the surface of Ni-sheathed NiO$_x$ nanoparticles can be summarized as a sequence consisting of four reactions: 1) after organic substrate degradation in the anodic chamber, the generated protons are reduced by NiO$_x$ nanoparticles (Reaction 1); 2) this is followed by the oxygen adsorption reaction, in which each oxygen molecule adsorbs onto two adjacent NiOOH of the cathode surface, forming the bridged adsorption sites; 3) next, an electron-transfer step occurs (Reaction 3), which represents the rate-determining step of the ORR reactions; and 4) finally, the Oads species are reduced (Reaction 4) and water is produced as the final product. This sequence is the four-electron pathway.

Reaction 1: $NiO_x + H^+ + e^- \rightarrow NiO_{x-1}OH$

Reaction 2: $2NiO_{x-1}OH + O_2 \rightarrow [(NiO_{x-1}OH)O_{ads}]_2$

Reaction 3: $[(NiO_{x-1}OH)O_{ads}]_2 + H^+ + e^- \rightarrow (NiO_{x-1}OH)O_{ads} + H_2O + NiO_x$

Reaction 4: $(NiO_{x-1}OH)O_{ads} + H^+ + e^- \rightarrow H_2O + NiO_x$
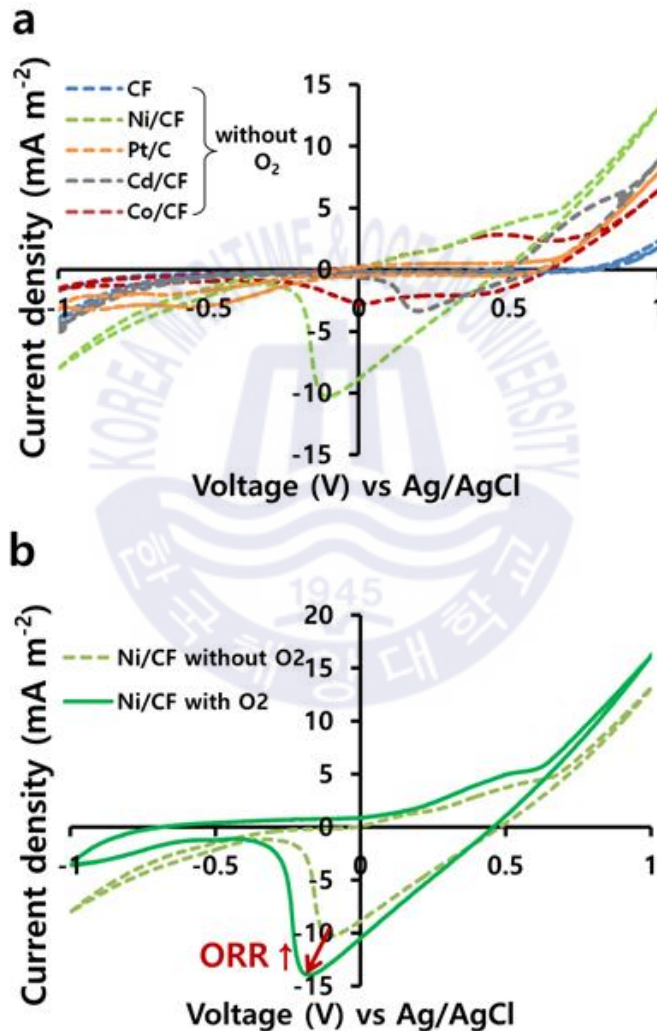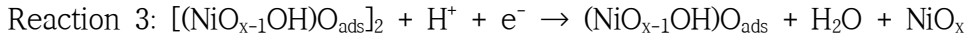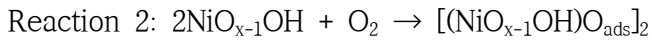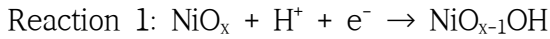
Fig. 2.4. (a) CV curves of the investigated PGM-free catalyst cathodes in 1 M of NaOH at 50 mV s^{-1} scan rate at room temperature and (b) ORR catalytic activity of the Ni/CF cathode under oxygen injection.

2.3.4. Open circuit voltage and power density

The performance of the various fabricated PGM-free catalysts were investigated in a single-chamber air-cathode MFC under batch mode conditions, as shown in Fig. 2.5. As shown in the figure, Ni/CF exhibited the highest OCV value (0.762 V) compared to other investigated cathode catalyst materials, for which the obtained OCV values were 0.762, 0.538, 0.524, and 0.405 V for the MFCs based on Ni/CF, Pt/C, Cd/CF, and Co/CF, respectively, (Fig. 2.5a).

Fig. 2.5b shows the generated power density of the MFCs based on the fabricated PGM-free cathode catalysts. A significant increase in the produced power was observed in the case of Ni/CF cathode, where, the maximum produced power density of MFCs were 1630.7 (Ni/CF), 489.6 (Pt/C), 125.3 (Cd/CF), and 76.3 mW m^{-2} (Co/CF), respectively. This increase in the produced power density based on a Ni/CF electrode is attributed to the formation of homogeneous Ni-sheathed NiO_x nanoparticles layers on the surface of the pristine CF cathode material. These layers act as efficient catalysts by decreasing the charge transfer resistance, increasing the surface area, enhancing the active sites, and improving the surface wettability of the pristine CF cathode material.

As shown by the current density for MFCs based on the fabricated PGM-free catalysts, the Ni/CF cathode exhibited a 250% greater current density compared to that achieved by the Pt/C commercial cathode catalyst material. The produced current densities were 9296.6, 3809.4, 964.2, and 819.2 mA m^{-2} for Ni/CF, Pt/C, Cd/CF, and Co/CF, respectively. This result further confirms the effectiveness of the Ni-sheathed NiO_x nanoparticles as a catalyst layer for enhancement of cathode performance and to increase the produced current and power densities of MFCs. On the other hand, it can be clearly observed from Fig. 2.5c that the produced current density for all investigated

MFCs based on the various fabricated cathode materials started at maximum values and then decreased with time until a stable state was reached. This sharp decrease in the initial current density is due to the rapid depletion of accumulated electrons on the anode surface during MFC operation.

Anode and cathode potentials were recorded over time during MFC tests. As shown in the figure, the anodes potential changed slightly with time because of the accumulation of produced electrons generated by the exoelectrogenic reactions in the anodic chamber. This is in contrast to the cathodes potential which changed significantly with time. This change in cathodes potentials is mostly due to the high catalytic activity and chemical stability of the catalyst materials with respect to ORR reactions. However, the Ni/CF cathode exhibited the greatest stability in electrode potential compared to the other electrodes, thereby confirming the high catalytic stability of Ni-sheathed NiO_x nanoparticles with respect to the ORR reaction.

Therefore, it can be concluded that the performance of an MFC can be greatly enhanced by using Ni-sheathed NiO_x as cathode catalyst layer. This is due to the combination of high metallic activity and electrical conductivity of Ni, together with the high electrocatalytic activity of NiO_x with respect to the ORR (four-electron pathway reactions), which results in the enhancement of electron transfer, a decrease in charge transfer resistance, and an increase in the generated current and power densities of MFCs.

Notably, and in contrast to previous studies, the introduced Ni/CF cathode material exhibited higher current and power densities compared to that obtained in previous studies (as shown in Table 2.1). This indicated that the Ni/NiO_x nanoparticle is a superior electroactive catalyst material for ORR in single air-cathode MFCs operated in the batch mode.
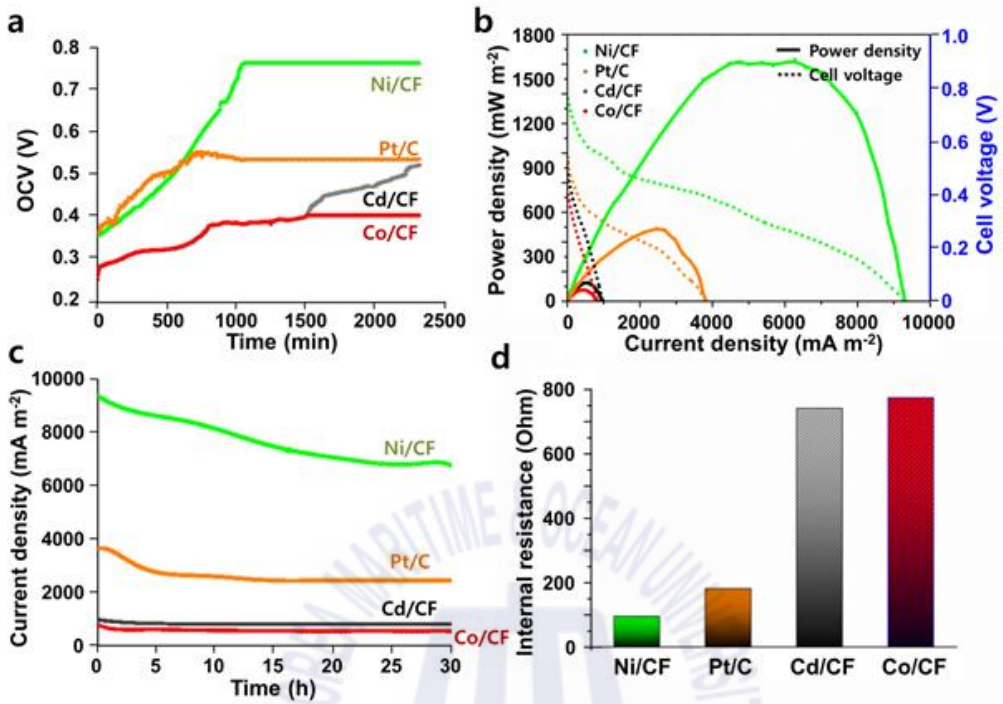
Fig. 2.5. (a) Open circuit voltage versus time during MFC experiments, (b) polarization curve, (c) current stability, and (d) internal resistance of MFCs based on pristine and fabricated PGM-free catalyst cathodes.

Table 2.1. Maximum power density of air-cathode MFC based on catalysts doped carbonaceous cathode materials using different fabrication techniques.

Cathode	Preparation method	Morphology	Power density ($mW \cdot m^{-2}$)	Reference
Ni/CF	Electrophoresis	Nanoparticles	1630.7	This study
Pt/C			489.6	
Cd/CF			125.3	
Co/CF			76.32	
Ni/C	Settling and applying	Nanoparticles	26.0	[43]
NiCNF/ACF	Chemical vapor deposition	Fibers	600	[26]
Ni/C	Brushing	Nanoparticles	94.4	[28]
$MnCo_2$	Thermal treatment	Filamentous shape	113	[44]
Mn-PPY-CNT	Solvothermal	Wires	213	[45]
CPs	Polymerization	Nanoparticles	122	[46]
Co_3O_4	Hydrothermal	Nano flakes	347	[27]
Pt_7Sn_3P/C	Impregnation	Nanoparticles	361	[19]
Pt_7Sn_3/C			336	
Sn/C			108	
Pt_3Sn_7/C			207	
Pt_5Sn_5/C			245	
α-MnO_2	Hydrothermal	Nanowires	111	[47]
α-MnO_2/C			180	
AC-E20	Heating	Layers	1070	[48]

Cathode	Preparation method	Morphology	Power density (mW m^{-2})	Reference
3wt% Co$_3$O$_4$/NiCo$_2$O$_4$DSNC	Rolling-press	Yolk-shelled layers	1433	[49]
7wt% Co$_3$O$_4$/NiCo$_2$O$_4$DSNC			1230	
Fe-AAPyr	Pyrolysis	Layers	1300	[50]

CF: carbon felt; CNF: carbon nanofiber; Mn-PPY-CNT: manganese-polypyrrole-carbon nanotube; CPs: carbon powders; CoTMPP: Co-tetra-methyl phenyl porphyrin; AC-E20: enrofloxacin; DSNC: double-shelled Nano cage; Fe-AAPyr: iron amino-anti pyrine.

2.3.5 Internal resistance of MFCs

The overall internal resistance of the MFC means the resistance of ions to flow through the proton exchange membrane as well as the electrolytes, in addition to the resistance of electrons to transfer through the electrodes and interconnections [35, 36]. This internal resistance can be calculated from the slope of the linear polarization curve (Fig. 2.5a).

Figure 2.5d shows the internal resistances of the MFC based on PGM-free catalyst cathode materials. As shown by Fig. 2.5d, the Ni/CF cathode material exhibited the lowest internal resistance (96.3 Ω) compared to Pt/C, Cd/CF, and Co/CF cathode materials, which achieved values of 181.9, 754.8, and 771.9 Ω, respectively. These results demonstrate the positive effect of the metal-sheathed metal oxide nanoparticle layers, which act as efficient catalysts, decreasing the charge transfer resistance and enhancing the generated current and power densities.

2.3.6 COD removal and coulombic efficiency

Figure 2.6 shows the COD removal and CE percentage of the MFCs based on the different fabricated cathode catalyst materials. As shown, the COD removal was higher than 50% for all utilized cathodes, which confirms the high potential of MFC technology for wastewater treatment. COD removal was 78.4, 69.8, 60.5, and 54.2% for an MFC based on Ni/CF, Pt/C, Cd/CF, and Co/CF cathodes, respectively. Furthermore, the ratio of the produced current densities to the oxidized organic substrates has been calculated using the CE equation, as shown in Fig. 2.6 (dash columns). The Ni/CF cathode material exhibited the highest CE (84.1%), compared to the Pt/C, Cd/CF, and Co/CF cathodes. The achieved CE values were 49.6, 38.8, and 25.0% for the Pt/C, Cd/CF, and Co/CF cathodes, respectively.
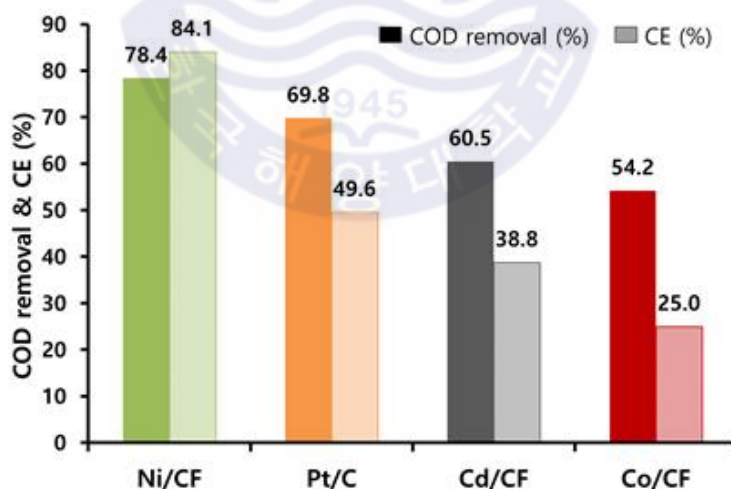
Fig. 2.6. COD and coulombic efficiency of MFCs based on fabricated PGM-free catalyst cathodes.

2.4. Conclusions

Nickel (Ni), Cadmium (Cd), and Cobalt (Co) nanoparticles were successfully synthesized on the surface of CF as a carbonaceous cathode material using a simple EPD technique. Due to the high activity of Ni metals, the synthesized Ni nanoparticles were covered by a thin layer of NiO_x. The nanostructure of the Ni/NiO_x strongly enhanced the electrochemical activity with respect to ORR in the four-electron pathway at a neutral pH. The maximum power density of an MFC based on the Ni/CF catalyst was four times greater than that obtained for MFCs based on a Pt/C catalyst under the same conditions. The high electrical conductivity of Ni coupled with the high catalytic activity of NiO_x, leads to an increase in the produced power and current densities of the MFCs. This is in addition to significant enhancements with respect to pollutant removal and coulombic efficiency. The super electrocatalytic activity and high durability for oxygen reduction means that the Ni/NiO_x nanoparticles are both attractive and efficient alternative cathode catalysts for use in MFCs.

2.5 references

[1] Tamilarasan K, Banu JR, Jayashree C, Yogalakshmi KN, Gokulakrishnan K. Effect of organic loading rate on electricity generating potential of upflow anaerobic microbial fuel cell treating surgical cotton industry wastewater. J Environ Chem Eng. 2017;5:1021-6.

[2] Jayashree C, Tamilarasan K, Rajkumar M, Arulazhagan P, Yogalakshmi KN, Srikanth M, et al. Treatment of seafood processing wastewater using upflow microbial fuel cell for power generation and identification of bacterial community in anodic biofilm. J Environ Manage. 2016;180:351-8.

[3] Jayashree C, Arulazhagan P, Adish Kumar S, Kaliappan S, Yeom IT, Rajesh Banu J. Bioelectricity generation from coconut husk retting wastewater in fed batch operating microbial fuel cell by phenol degrading microorganism. Biomass Bioenergy. 2014;69:249-54.

[4] Chae K-J, Choi M-J, Lee J-W, Kim K-Y, Kim IS. Effect of different substrates on the performance, bacterial diversity, and bacterial viability in microbial fuel cells. Bioresour Technol. 2009;100:3518-25.

[5] Du Z, Li H, Gu T. A state of the art review on microbial fuel cells: a promising technology for wastewater treatment and bioenergy. Biotechnol Adv. 2007;25:464-82.

[6] Sun Y, Duan Y, Hao L, Xing Z, Dai Y, Li R, et al. Cornstalk-derived nitrogen-doped partly graphitized carbon as efficient metal-free catalyst for oxygen reduction reaction in microbial fuel cells. Am Chem Soc. 2016;8:25923-32.

[7] Yang J, Zhou M, Zhao Y, Zhang C, Hu Y. Electrosorption driven by microbial fuel cells to remove phenol without external power supply. Bioresour Technol. 2013;150:271-7.

[8] Rozendal RA, Hamelers HV, Rabaey K, Keller J, Buisman CJ. Towards practical implementation of bioelectrochemical wastewater treatment. Trends Biotechnol. 2008;26:450-9.

[9] Larrosa-Guerrero A, Scott K, Head I, Mateo F, Ginesta A, Godinez C. Effect of temperature on the performance of microbial fuel cells. Fuel. 2010;89:3985-94.

[10] Behera M, Murthy SS, Ghangrekar MM. Effect of operating temperature on performance of microbial fuel cell. Water Sci Technol. 2011;64:917-22.

[11] Torres CI, Kato Marcus A, Rittmann BE. Proton transport inside the biofilm limits electrical current generation by anode-respiring bacteria. Biotechnol Bioeng. 2008;100:872-81.

[12] Kim BH, Chang IS, Gadd GM. Challenges in microbial fuel cell development and operation. Appl Microbiol Biotechnol. 2007;76:485.

[13] Mohamed HO, Sayed ET, Obaid M, Choi Y-J, Park S-G, Al-Qaradawi S, et al. Transition metal nanoparticles doped carbon paper as a cost-effective anode in a microbial fuel cell powered by pure and mixed biocatalyst cultures. Int J Hydrogen Energy. 2018;43:21560-71.

[14] Farahani FS, Mecheri B, Majidi MR, de Oliveira MAC, D'Epifanio A, Zurlo F, et al. MnO x-based electrocatalysts for enhanced oxygen reduction in microbial fuel cell air cathodes. J Power Sources. 2018;390:45-53.

[15] Cristiani P, Carvalho ML, Guerrini E, Daghio M, Santoro C, Li B. Cathodic and anodic biofilms in Single Chamber Microbial Fuel Cells. Bioelectrochemistry. 2013;92:6-13.

[16] Rasmussen M, Abdellaoui S, Minteer SD. Enzymatic biofuel cells: 30 years of critical advancements. Biosens Bioelectron. 2016;76:91-102.

[17] Santoro C, Babanova S, Erable B, Schuler A, Atanassov P. Bilirubin

oxidase based enzymatic air-breathing cathode: Operation under pristine and contaminated conditions. Bioelectrochemistry. 2016;108:1-7.

[18] Yuan H, Hou Y, Abu-Reesh IM, Chen J, He Z. Oxygen reduction reaction catalysts used in microbial fuel cells for energy-efficient wastewater treatment: a review. Mater Horiz. 2016;3:382-401.

[19] Li B, He Z, Wang M, Wang X. PtSnP/C and PtSn/C as efficient cathode catalysts for oxygen reduction reaction in microbial fuel cells. Int J Hydrogen Energy. 2017;42:5261-71.

[20] Yang W, Kim K-Y, Saikaly PE, Logan BE. The impact of new cathode materials relative to baseline performance of microbial fuel cells all with the same architecture and solution chemistry. Energy & Environmental Science. 2017;10:1025-33.

[21] Santoro C, Serov A, Stariha L, Kodali M, Gordon J, Babanova S, et al. Iron based catalysts from novel low-cost organic precursors for enhanced oxygen reduction reaction in neutral media microbial fuel cells. Energy Environ Sci. 2016;9:2346-53.

[22] Santoro C, Serov A, Narvaez Villarrubia CW, Stariha S, Babanova S, Schuler AJ, et al. Double-Chamber Microbial Fuel Cell with a Non-Platinum-Group Metal Fe-N-C Cathode Catalyst. ChemSusChem. 2015;8:828-34.

[23] Wen Q, Wang S, Yan J, Cong L, Pan Z, Ren Y, et al. MnO2-graphene hybrid as an alternative cathodic catalyst to platinum in microbial fuel cells. J Power Sources. 2012;216:187-91.

[24] Deng L, Zhou M, Liu C, Liu L, Liu C, Dong S. Development of high performance of Co/Fe/N/CNT nanocatalyst for oxygen reduction in microbial fuel cells. Talanta. 2010;81:444-8.

[25] Singh S, Verma N. Fabrication of Ni nanoparticles-dispersed carbon

micro-nanofibers as the electrodes of a microbial fuel cell for bio-energy production. Int J Hydrogen Energy. 2015;40:1145-53.

[26] Modi A, Singh S, Verma N. Improved performance of a single chamber microbial fuel cell using nitrogen-doped polymer-metal-carbon nanocomposite-based air-cathode. Int J Hydrogen Energy. 2017;42:3271-80.

[27] Kumar R, Singh L, Zularisam AW. Mesoporous Co3O4 nanoflakes as an efficient and non-precious cathode catalyst for oxygen reduction reaction in air-cathode microbial fuel cells. J Taiwan Inst Chem Eng. 2017;78:329-36.

[28] Ghasemi M, Daud WRW, Rahimnejad M, Rezayi M, Fatemi A, Jafari Y, et al. Copper-phthalocyanine and nickel nanoparticles as novel cathode catalysts in microbial fuel cells. Int J Hydrogen Energy. 2013;38:9533-40.

[29] Thapa B, Seetharaman S, Chetty R, Chandra TS. Xerogel based catalyst for improved cathode performance in microbial fuel cells. 2019.

[30] Mohamed HO, Abdelkareem MA, Obaid M, Chae S-H, Park M, Kim HY, et al. Cobalt oxides-sheathed cobalt nano flakes to improve surface properties of carbonaceous electrodes utilized in microbial fuel cells. Chem Eng J. 2017;326:497-506.

[31] Logan BE. Microbial fuel cells: John Wiley & Sons; 2008.

[32] Huang Q, Zhou P, Yang H, Zhu L, Wu H. In situ generation of inverse spinel CoFe2O4 nanoparticles onto nitrogen-doped activated carbon for an effective cathode electrocatalyst of microbial fuel cells. J Chem Eng. 2017;325:466-73.

[33] Sudhasree S, Shakila Banu A, Brindha P, Kurian GA. Synthesis of nickel nanoparticles by chemical and green route and their comparison in respect to biological effect and toxicity. Toxicol Environ Chem. 2014;96:743-54.

[34] Kulkarni A, Pratap R. X-ray diffraction study of epitaxial zinc and

cadmium films prepared by hot-wall technique. Mater Sci. 1986;8:449-52.

[35] Caffarena VdR, Capitaneo JL, Simão RA, Guimarães AP. Preparation of electrodeposited cobalt nanowires. Mater Res. 2006;9:205-8.

[36] Yuan X, Hu X-X, Ding X-L, Kong H-C, Sha H-D, Lin H, et al. Effects of cobalt precursor on pyrolyzed carbon-supported cobalt-polypyrrole as electrocatalyst toward oxygen reduction reaction. Nanoscale Res Lett. 2013;8:478.

[37] Usachov DY, Dobrotvorskii A, Shikin A, Adamchuk V, Varykhalov AY, Rader O, et al. Graphene morphology on Ni single-crystal surfaces: Experimental and theoretical investigation. Bull Russ Acad Sci. 2009;73:679-82.

[38] Zahariev I, Piskin M, Karaduman E, Ivanova D, Markova I, Fachikov L. FTIR spectroscopy method for investigation of Co-Ni nanoparticle nanosourface phenomena. J Chem Technol Metall. 2017;52.

[39] Wei L, Yuan D. The Nano-Electrocatalysts for Rechargeable Zinc Air Batteries. J Nanosci Nanotechnol. 2018;2.

[40] Wang Q, Cai Z, Huang L, Pan Y, Quan X, Puma GL. Intensified degradation and mineralization of antibiotic metronidazole in photo-assisted microbial fuel cells with Mo-W catalytic cathodes under anaerobic or aerobic conditions in the presence of Fe (III). Chem Eng J. 2018.

[41] Gebresemati M, Das G, Park BJ, Yoon HH. Electricity production from macroalgae by a microbial fuel cell using nickel nanoparticles as cathode catalysts. Int J Hydrogen Energy. 2017;42:29874-80.

[42] Artyushkova K, Serov A, Rojas-Carbonell S, Atanassov P. Chemistry of multitudinous active sites for oxygen reduction reaction in transition metal-nitrogen-carbon electrocatalysts. J Phys Chem C. 2015;119:25917-28.

[43] Liu J, Vipulanandan C. Effects of Fe, Ni, and Fe/Ni metallic nanoparticles

on power production and biosurfactant production from used vegetable oil in the anode chamber of a microbial fuel cell. Waste Manage (Oxford). 2017;66:169-77.

[44] Mahmoud M, Gad-Allah TA, El-Khatib KM, El-Gohary F. Power generation using spinel manganese-cobalt oxide as a cathode catalyst for microbial fuel cell applications. Bioresour Technol. 2011;102:10459-64.

[45] Lu M, Guo L, Kharkwal S, Wu Hn, Ng HY, Li SFY. Manganese-polypyrrole-carbon nanotube, a new oxygen reduction catalyst for air-cathode microbial fuel cells. J Power Sources. 2013;221:381-6.

[46] Zhong S, Zhou L, Wu L, Tang L, He Q, Ahmed J. Nitrogen-and boron-co-doped core-shell carbon nanoparticles as efficient metal-free catalysts for oxygen reduction reactions in microbial fuel cells. J Power Sources. 2014;272:344-50.

[47] Majidi MR, Shahbazi Farahani F, Hosseini M, Ahadzadeh I. Low-cost nanowired α-MnO2/C as an ORR catalyst in air-cathode microbial fuel cell. Bioelectrochemistry. 2019;125:38-45.

[48] Liu W, Cheng S, Sun D, Huang H, Chen J, Cen K. Inhibition of microbial growth on air cathodes of single chamber microbial fuel cells by incorporating enrofloxacin into the catalyst layer. Biosens Bioelectron. 2015;72:44-50.

[49] Zhang S, Su W, Li K, Liu D, Wang J, Tian P. Metal organic framework-derived Co3O4/NiCo2O4 double-shelled nanocage modified activated carbon air-cathode for improving power generation in microbial fuel cell. J Power Sources. 2018;396:355-62.

[50] Gajda I, Greenman J, Santoro C, Serov A, Melhuish C, Atanassov P, et al. Improved power and long term performance of microbial fuel cell with Fe-N-C catalyst in air-breathing cathode. Energy. 2018;144:1073-9.

Chapter 3.

Electrophoretically fabricated nickel/nickel oxides as cost effective nanocatalysts for the oxygen reduction reaction in air-cathode microbial fuel cell

3.1 Introduction

Microbial electrolysis cells (MECs) are technologies that produce high value-added materials such as hydrogen, methane, ethanol, and butanol from organic matter in wastewater by electroactive microorganisms (exoelectrogens) [1-3]. In other words, MEC has two advantages: wastewater treatment and efficient energy production. Among the main materials that MEC can produce, hydrogen has been selected as the main target material because it does not emit pollutants (greenhouse gas) when used as fuel [4]. The two-chambered MEC for hydrogen production is separated into two spaces using the cation exchange membrane and is composed of the anode and the cathode, respectively [5]. In the anode chamber, various microorganisms called anode-respiring bacteria (ARB) grow and oxidize soluble organics in wastewater to generate H+, e^-, and CO_2 [6]. The generated electrons and hydrogen ion transport to the cathode through the external circuit and PEM, and they are reduced to H2 gas at the cathode.

Among the elements that make up the MEC, especially the anode is an important part of the MEC because the ARB effectively transfers the charge from the microorganism-anode interface to the anode by increasing the microbial density [7, 8]. It is essential to concentrate the ARB on the anode and accelerate the electron transfer rate to achieve high performance. Thus,

carbon-based materials (e.g., carbon felt [9], carbon paper [10], graphite [11], and granular activated carbon (GAC) [12]) having low cost, high durability, electrical conductivity, and high surface area have been mainly selected. Among them, 3D porous carbon structures such as carbon felt, carbon sponge, and carbon foam has been widely used in microbial bioelectrochemical systems due to its large bio-accessible area [13, 14]. However, the unique hydrophobicity of the carbon-based structure is incompatible with the strong microbial adhesive surface due to bacterial activity and electron transfer defects by preventing moisture penetration and gas release inside the carbon felt [15-17]. In other words, it is limited to the 2D role even though it is a material having a high surface area using only the electrode surface without using the entire area of carbon felt.

To solve these problems, recently, research results using the anode by coating carbon nanotubes or conductive polymers such as polyaniline, and polypyrrole to increase the density of current generating microorganisms of inefficient porous carbon-based materials have been reported in microbial electrochemical system [18-20]. Cui et al. electropolymerized polyaniline (PANI) on the surface of large porous graphite felt (GF), followed by electrophoretic deposition of carbon nanotubes (CNT). MFC maximum power densities from CNT-125/PANI/GF (308 mW m^{-2}) anodes increased by 628% and 385% compared to those from the original GF (49 mW m^{-2}) and PANI/GF (80 mW m^{-2}), respectively [21]. Feng at el. fixed the Shewanella decolorationis S12 using polypyrrole/anthraquinone-2,6-disulphonic disodium salt (PPy/AQDS)/CF modified anode and showed that the maximum power density of the two-chambered MFC was 1303 mW m^{-2} [22].

Among the conductive polymers, Poly (3, 4-ethylenedioxythiophene) polystyrene sulfonate (PEDOT:PSS) is commonly used material as a display, biosensor, and medical device because of its high electrical conductivity ,

biocompatible, excellent stability, and good processability [23-25]. When present in an oxidized state after oxidation polymerization, PEDOT:PSS has a high conductivity by polaron or bipolaron [26]. PEDOT is still hydrophobic, but PEDOT:PSS is hydrophilic because hydrophilic PSS is polymerized while surrounding the outside of PEDOT [27]. PEDOT has positive charge and PSS has SO^{-3} negative charge, so it is combined through strong electrical interaction (attractive force) and has excellent stability [28]. These characters of PEDOT:PSS are well-matched with anodes of BES and has recently emerged as a novel electrode material to improve the performance of BES. For example, conductive PEDOT:PSS films were coated on CF anodes and inoculated in palm oil mill waste to show good biocatalytic performance when catalyzing acetate metabolism [29]. Zajdel et al. developed a multi-layered conductive bacterial composite film (MCBF) produced by inserting S. oneidensis into PEDOT:PSS and co-immobilized on a porous CF substrate, showing a 20-fold increase in current compared to CF [30]. These studies present the key possibility that surviving exoelectrogens across 3D porous PEDOT:PSS/CF increases bacterial density, current production and maximizes hydrogen production from the MEC to the anode. Especially, the conductivity polymer-doped 3D porous anode has been applied to MFC, and there is no performance verification for MEC. In addition, it is necessary to analyze detaily the microbiological deposition and electrical characteristics according to the depth of the electrode.

In this study, PEDOT:PSS, a unique super-hydrophilic material with both conductivity and biocompatibility, was used to improve electron transfer capacity of anodes. The electrode modification method using electropolymerization is very simple, and the physicochemical and electrical properties of the modified electrodes were evaluated. The scope of this study provides new insights into the BES by increasing the potential of the anode

using materials that were not used in MEC.

3.2 Materials & methods

3.2.1 Preparation of PEDOT:PSS doped carbon felt

Carbon felt (CF, 5 × 5 cm, 50 mm thickness, purchased from Morgan, UK) was soaked in 50% nitric acid for 12 s followed by drying all night to remove impurity and improve hydrophilicity. It was attached to an electron collector made of stainless steel with silver paste and pressed for 1 day with a weight of 1 kg.

3, 4-Ethylenedioxythiophene (EDOT) 97% and Poly(sodium 4-styrenesulfonate) (NaPSS) purchased from Sigma-Aldrich were prepared for electropolymerization. Lithium chloride (LiClO4) 95% purchased from Sam-Chun was used as electrolyte. The pretreated CF was impregnated into the mixed solution (DI water; 19.5 mL, $LiClO_4$; 0.0112 g; EDOT 0.5 mL; and NaPSS 0.801 g). Subsequently, galvanostat (ZIVE SP1, WonATech, Korea) was used to coat by electropolymerization at 100 mA in galvanic mode for 12 hours; Graphite, CF, and Pt wire were selected as the counter electrode, working electrode, and reference electrode, respectively. The PEDOT:PSS doped CF electrode (PEDOT:PSS/CF) dried overnight after electropolymerization was put into deionized water for 1 day and heat treated at 110℃ for increased durability.

3.2.2 Morphology and biocompatibility property

The surface morphology of the fabricated anodes before and after application to the MEC was investigated by field emission scanning electron

microscopy (FE-SEM, Czech Republic). After obtaining sufficient hydrogen production data from MEC, the morphology of bacteria attached to the anode was investigated. The electrode detached from the MEC was cut into 1×1 cm pieces and the height of the electrode was divided into two parts in order to confirm the presence of bacteria inside the electrode. After that, these were washed with pH7 phosphate buffer. To remove moisture and fix the form of microorganisms, the specimens were immersed in glutaraldehyde (2.5% final, Sigma-Aldride, USA) for 1 h, washed three times with DI Water, and then performed in the equal method for Osmium (1% final, Sigma-Aldride, USA). Subsequently the specimens were dehydrated twice each in a series of graded aqueous ethanol solutions (50, 70, 80, 90, 95, and 100%) for 10 minutes each. The pretreated electrodes were dried overnight at room temperature. Prior to SEM observation, the ssmples were coated with platinum for 60 sec at 15 mA using ion sputtering (E-1030, Hitachi Ltd., Japan). The element compositions was figured out with an energy dispersive X-ray (EDX) attached to FE-SEM.

3.2.3 Chemical structure and wettability

The functional group of the prepared anode was analyzed using Raman spectroscopy (JASCO, NRS-5100, Japan) with laser excitation at 532 nm in the range of 700–4200 cm^{-1}. The elements structure were analyzed using Fourier-transform infrared spectroscopy (FT-IR, Spectrum GX, Perkin Elmer, USA) in the wave number range of 650–4000 cm^{-1} under the ATR mode.

The hydrophilicity was determined by dropping 6 μL of deionized water at 1 sec intervals onto the pristine CF and fabricated PEDOT:PSS/CF each other, and the value of water contact angle (WCA, DSA25, Kruss, germany) was recorded at room temperature.

3.2.4 Electrochemical analysis

The electrocatalytic activity of the prepared cathode materials was investigated using cyclic voltammetry (CV) and impedance spectroscopy (EIS) (ZIVE SP1, WonATech, Korea) in a three-electrode cell. In which, the fabricated PEDOT:PSS/CF electrode was connected as the working electrode, whereas Ag/AgCl and a Pt wire were used as the reference and counter electrodes. CV was tested at −1–1 V with 50 mV sec^{-1} in phosphate buffer solution pH7 with nitrogen gas purging to remove oxygen for anaerobic condition. The CV was performed for 5 cycles and was obtained in the last cycle. EIS measurement was set to the same condition as CV, recorded in the range of 0.01 Hz to 100 kHz, and the amplitude was 10 mV.

3.2.5 Two-chambered MEC set-up and operation

The pristine CF (control) and fabricated PEDOT:PSS/CF were applied to a two-chamber MEC producing hydrogen to compare the actual MEC performance. It consists of anode chamber (working volume 140 mL + headspace 50mL) and cathode chamber (working volume 165 mL + headspace 50 mL) separated with Nafion 117 membrane (7 × 7 cm, DuPont, USA). The anodes were applied differently with pristine CF and PEDOT:PSS/CF, respectively, while cathodes were used equally with the Pt-rod perforated titanium plate (0.5 mg Pt cm^{-2}). Nutrient mineral buffer (NMB) solution was added as anolyte to support microorganism growth and anaerobic digestion sludge (mixed culture) from Soo-young wastewater treatment plant was used as microbial inoculum. The phosphate buffer pH7 was filled as catholyte in the cathode chamber. Acetic acid (1.5 mM) was injected as the substrate after purging headspace with nitrogen every batch. The injected acetate was

assumed to be completely consumed during the first cycle of batch testing. Hydrogen production efficiency was compared using a MEC equipped with test electrodes (CF vs. PEDOT:PSS/CF) after 3 months of preliminary stabilization. Gas production and composition analysis were performed by taking a gas sample (0.5 mL) from a MEC headspace using an airtight syringe (2.5 mL, Hamilton SampleLock Syringe♯ 1002, USA) and performing gas chromatography (GC, Series 580, GawMac Instrument Co., USA). Hydrogen production rate was detected by respirometer (BRS-110, EETech, Korea). To initiate hydrogen production, an external voltage of 0.7 V was applied to the MEC using a DC power source. All prepared reactors were operated in an incubator at 30℃ under 350 rpm.

3.2.6 Coulombic efficiency

The actual energy production efficiency of MEC due to the decomposition of organic substrates by microorganisms was calculated using the following coulomb efficiency (eqn. (3)).

$$CE = \frac{M \int_0^t I dt}{F b V_{am} \Delta COD}$$

(3)

where M is the oxygen molecular weight (32 g mol^{-1}), F is Faraday's constant (96485 C mol^{-1}), b indicates the number of electrons exchanged per one oxygen molecule (4), V is the volume of the reactor. Current (I) which is connected with fixed resistance (10 Ω) on the cathode side was continuously monitored by a multimeter (Keithley 2700, USA). COD was measured before and after MFC experiments using an HS COD-LR kit (Humas, HS 2300 plus, Korea).

3.3 Results & Discussion

3.3.1 Morphology and elements of the fabricated anodes

FE-SEM images showed that the PEDOT:PSS thin layer was successfully deposited each carbon fiber (Fig. 3.1b) compared pristine CF (Fig. 3.1a). Surface roughness of PEDOT:PSS thin layer in PEDOT:PSS/CF increased after heat treatment (Fig. 3.1c), which enhanced surface area.

EDX also confirmed the presence of PEDOT:PSS on the PEDOT:PSS/CF surface. Unlike CF, where only carbon was detected, PEDOT:PSS/CF samples showed S peak (6.79%) from thiophene of PEDOT and SO^{-3} of PSS, and O peak (23.10%) by PEDOT. Little amount of Na (0.95%) corresponding to dopant (NaPSS) were observed. PEDOT:PSS/CF after heat treatment also showed S (17.09%), O (5.86%) element signal.
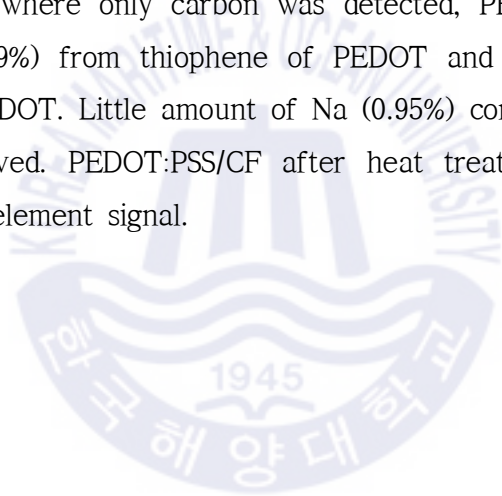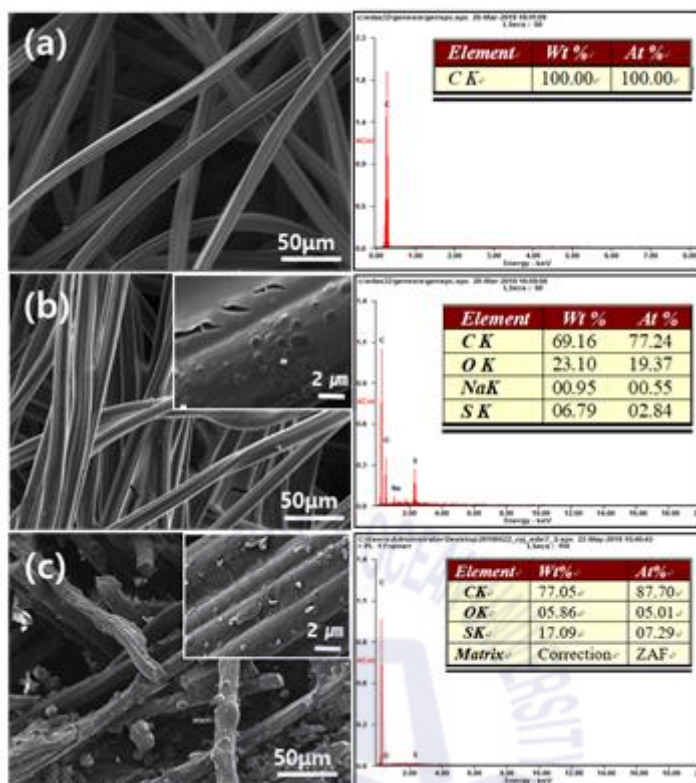
Fig. 3.1. FE-SEM images and EDX results of (a) CF, (b) PEDOT:PSS/CF in room temperature, and (c) PEDOT:PSS/CF after heat treatment.

3.3.2 Chemical structure of the fabricated anodes

Figure 3.2 shows Raman (Fig. 3.2a) and FT-IR (Fig. 3.2b) spectra for all prepared anode materials. Raman peaks of CF doped with CF, PEDOT:PSS/CF, and commercialized PEDOT:PSS solution physically coated CF (PEDOT:PSS-CF) were investigated to indicate polymerized form PEDOT:PSS rather than each PEDOT and PSS. The Raman spectrum of CF shows only wide two peaks witch can find typically in carbon materials; the D band peak (structure defects and disorders) generally located at 1358 cm^{-1} and the G band peak

- 52 -

(graphite) which is observed at about 1589 cm^{-1}. The peaks at 1003, 1269, 1361, and 1436 cm^{-1} in PEDOT: PSS/CF represent $C_\beta-C_\beta$' asymmetric vibration, $C_\alpha-C_\alpha$' inter-ring stretching vibration, $C_\beta-C_\beta$' stretching vibration, and the divisions of $C_\alpha=C_\beta$ symmetric stretching vibration, respectively [31, 32]. The peak at 1507 cm^{-1} corresponds to $C_\alpha=C_\beta$ asymmetric elongation vibration associated with the thiophene ring in the PEDOT chain [33]. The peak of PEDOT:PSS-CF was also observed in almost the same area, although it was not clear due to the two large peaks from CF. The Raman shift from 1440 cm^{-1} to 1436 cm^{-1}, after doping, indicates that the thiophene ring changes from $C_\alpha=C_\beta$ of benzoid structure to $C_\alpha-C_\beta$ of quinoid structure due to oxidation reaction [34]. In addition, a peak at 1565 cm^{-1} was found showing an apparent quinoid structure ($C_\alpha-C_\beta$) [35]. These results indicate the movement by the heat treatment process for 12 hours after the electropolymerization.

FT-IR was used to evaluate components with infrared absorption characteristics that are inactive in Raman. Commercial PEDOT:PSS solution was prepared by drying for one day without heat treatment and showed clear peaks comparison of pristine CF, PEDOT:PSS/CF. PEDOT:PSS/CF showed similar shape to commercial PEDOT:PSS peaks, unlike CF in the fingerprint range (1500 to 500 cm^{-1}). In the PEDOT:PSS/CF, 1716, 1654, and 1427 cm^{-1} peaks indicate the asymmetric stretching mode of $C_\alpha=C_\beta$, symmetric $C_\alpha=C_\beta$, and asymmetric $C_\alpha-C_\beta$ indicating quinoid structure of the thiophene ring, respectively [36, 37]. The 1334 cm^{-1} bands correspond to ring strains in the stretching mode of the ethylenedioxy (C-O-C) [38]. The weaker band of about 1137 cm^{-1} occurs due to stretching vibrations from the SO^{-2} or SO^{-3} groups of PSS [39]. The observed peak at 998 cm^{-1} (C-S) is derived from the stretching vibrations of thiophene ring [40]. The presence of the peak at 2875 cm^{-1} indicates C-H stretching bend [41]. Therefore, these results showed that

the coating of PEDOT:PSS was successfully achieved on the CF surface.
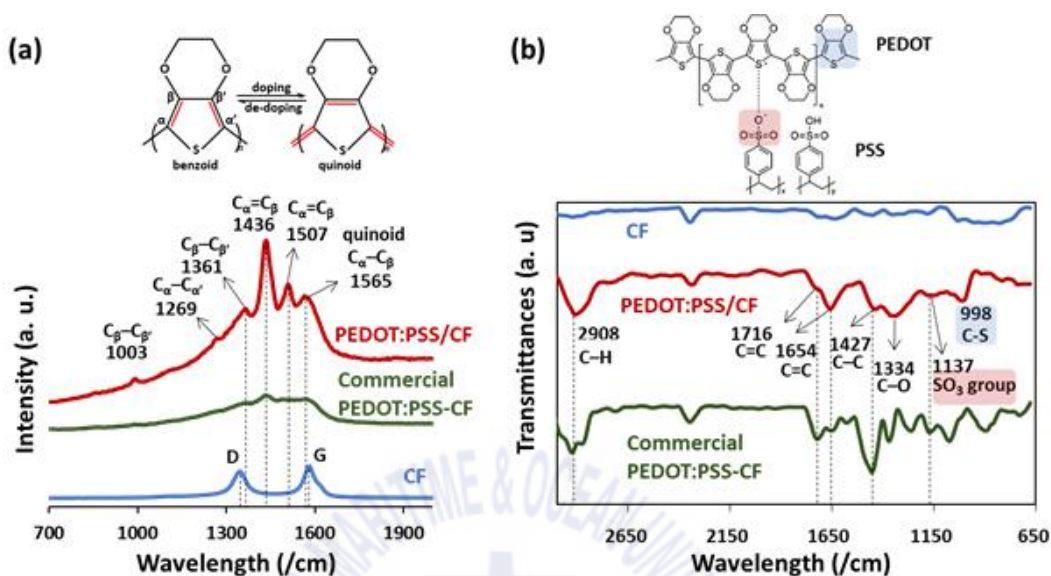
Fig. 3.2. (a) Raman spectrum and (b) FT-IR of pristine CF, fabricated
PEDOT:PSS/CF, and commercial PEDOT:PSS doped CF.

3.3.3 Wettability of fabricated electrodes

The hydrophilicity of the electrode material is a major factor in accelerating microbial adhesion growth and facilitating the release of the resulting biogas. The hydrophobicity of CF resists surface wetting by the organic solution, increasing the resistance of the electrode-microbial interface and preventing electron transfer to the electrode. In addition, hydrophobicity of CF can be further enhanced by capture of the produced biogas. The CF surface was converted from hydrophobic to super hydrophilic after PEDOT: PSS modification as shown in Fig. 3.3. The prepared electrodes were cut into two parts (outer region and inner region) to observe the wettability of the electrode surface and the inside. The water contact angle of CF is markedly

reduced from 113.6° to 0° for the PEDOT:PSS/CF electrode, indicating super-hydrophilic character. In addition, while the wettability inside the CF electrode showed hydrophobicity (123.3) compared to the outside, the wettability of PEDOT:PSS/CF still showed super-hydrophilicity (0). Therefore, the wettability results by electrode depth show that PEDOT:PSS is uniformly coated inside the electrode without film formation, resulting in improved electrode wettability over the entire area. It is expected that exoelectrogens will be attached to the entire area of the 3D porous PEDOT:PSS/CF electrode, resulting in higher hydrogen production rate and amount than CF due to improved electron transfer efficiency.
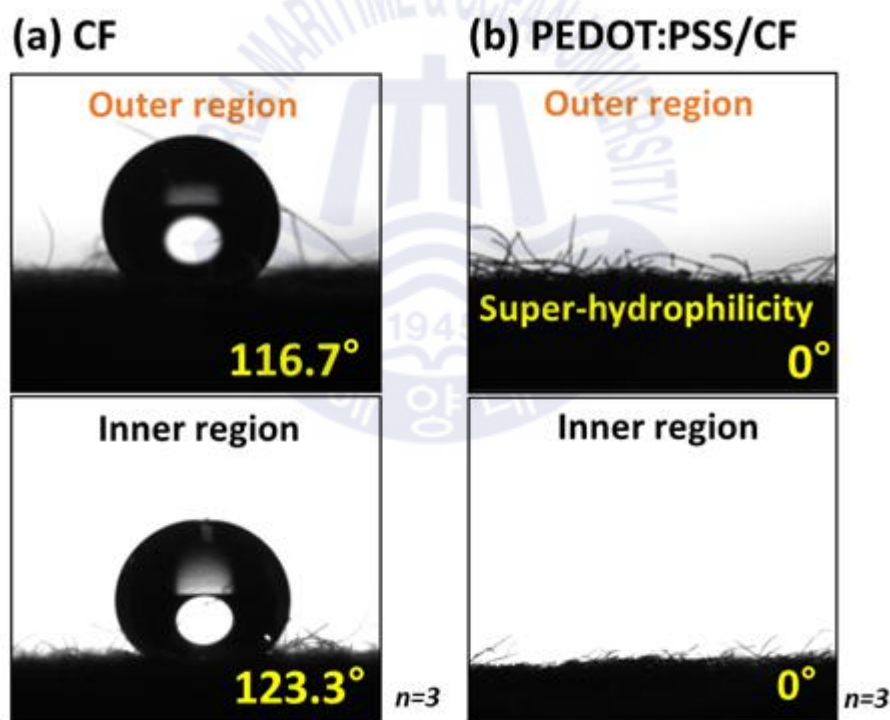
Fig. 3.3. Water contact angle of outer and inner region of (a) CF and (b) PEDOT:PSS/CF.

3.3.4 Electrical behavior of fabricated electrodes

Prepared CF and PEDOT:PSS/CF electrodes were divided into three parts according to the electrode depth and measured by the inside and outside of electrodes to see electrochemical behavior for whole area. Pristine CF and fabricated PEDOT:PSS/CF was measured in the range of −1 – 1 V using cyclic voltammetry (CV) to estimate the electrochemical activity (Fig. 3.4a). The PEDOT: PSS/CF (9.98 mA) electrode showed much higher capacitance currents than CF (4.17 mA) at the same specific voltage (0.37 V). Besides, the current densities of inside and outside part of the PEDOT: PSS/CF were similar. Thus, PEDOT:PSS was well deposited on the CF electrode even inside, which can provide greater active surface area for bacterial attachment and promote electrical conductivity.

The ideal anode has a very low charge transfer resistance (RCT) to ensure good electron transfer. Electrochemical impedance spectroscopy (EIS) was performed to determine the RCT value on the same conditions analyzed by CV. The trend of EIS data before and after electropolymerization shows a big difference between CF and PEDOT:PSS/CF. The inside and outside of the CF show a longer cafeteria resistance tail compared to PEDOT:PSS/CF, and the approximately 60° slope appears to be a greater factor for resistance to the electrical double layer. Nyquist plots outside and inside of PEDOT:PSS/CF (inset) showed much lower resistance compared to CF and had weak semicircles and tails showing capacitive and resistive contributions. Outside PEDOT:PSS/CF indicated a semicircle with a 2.5 times increase in RCT from 6.3 Ω to 16.2 Ω compared to the inside. However, the internal resistance, which represents the solution resistance and the resistance at the electrode−electrolyte interface, shows a similar trend. Besides, the small difference in resistance of the capacitor indicates that the PEDOT:PSS has

been sufficiently deposited to the interior.
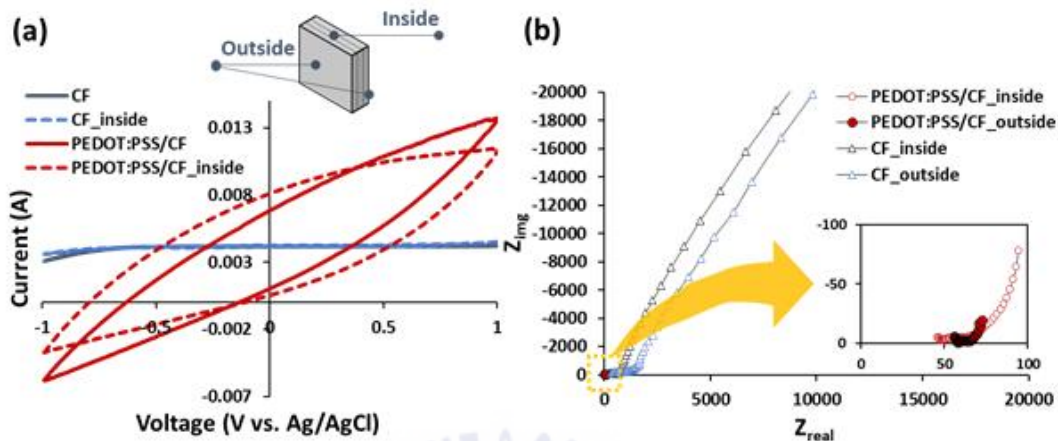
Fig. 3.4. (a) Cyclic voltammetry and (b) EIS of inside and outside of CF and PEDOT:PSS/CF.

3.3.5 MEC performance

In the anode chamber of MEC, methanogens grow competitively with exoelectrogens. The main growth of methanogens has a fatal effect on hydrogen production, since methane requires more electrons than hydrogen (electron equivalence: 8 mol e^- = 1 mol; CH_4 = 4 mol H_2, when acetate used as substrate). Therefore, inhibition of methangens and growth of exoelectrogen can improve target hydrogen production. The gas composition in the cathode chamber of the PEDOT:PSS/CF had higher hydrogen content (90.76%) than CF (82.43%) as shown in Fig. 3.5a. Hydrogen began to accumulate after about two months and was deployed four batch cycles earlier in PEDOT:PSS/CF compared to CF. Suspended sludge was removed and replaced with NMB to evaluate electrode performance and improve hydrogen purity (inhibition of methanogens). After removing suspended sludge, the

hydrogen content was higher in CF and PEDOT:PSS/CF, but there was no significant difference. It is believed that exoelectrogens adhered/grown more intensively on the electrode than dissolved sludge and inhibited the growth of methanogens.

The hydrogen production rate extracted from the anode side of the MEC was measured for final 3 batch cycles using the respirator as shown in Fig. 3.5b. The generated final hydrogen amount after completion of each batch reaction was 33.4% larger than the control in the reactor where PEDOT:PSS/CF was used. In addition, PEDOT:PSS/CF increased the hydrogen production rate by 1.65 times. Therefore, PEDOT:PSS is expected to promote the attachment of exoelectrogens, accelerate hydrogen production (rate) with high electrical conductivity (low resistance).
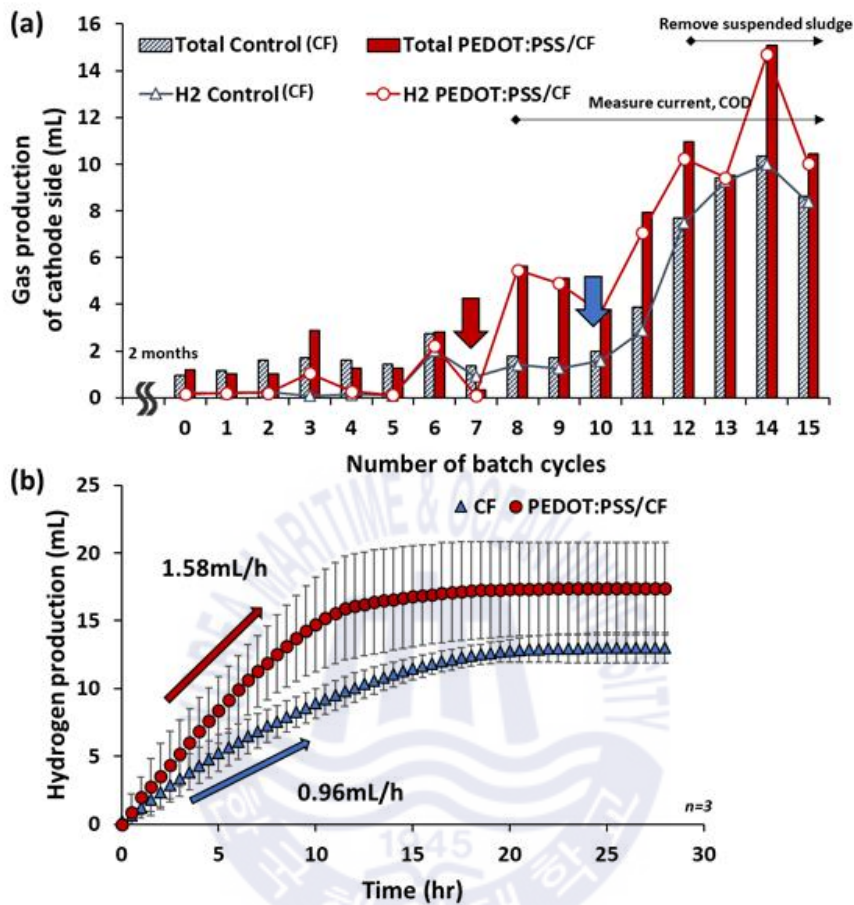
Fig. 3.5. (a) Gas production and (b) hydrogen production rate of cathode side of CF and PEDOT:PSS/CF.

3.3.6 Biocompatibility

Biocompatibility of biocatalysts and anode electrodes is an important factor in MEC development [14]. The manufactured PEDOT:PSS/CF anodes showed a stronger biofilm on the electrode surface and wall compared to untreated CF (Fig. 3.6a and b). The observed microorganisms showed the typical shape of

S. oneidensis, one of the most well-studied exoelectrogens [42]. S. oneidensis spreads not only on surfaces and cell walls, but also inside PEDOT:PSS/CF. In contrast, only a few S. oneidensis were observed inside the untreated CF anode. This suggested that the biocompatibility of the manufactured PEDOT:PSS/CF was superior to that of CF. Cai et al. reported biocompatibility and poor properties of CF. The excellent biocompatibility of the manufactured PEDOT:PSS/CF is due to the rough surface morphology and the hydrophilicity of PEDOT:PSS, which allows for greater active surface area for bacterial formation, promoting more active biomass adhesion [17]. The groups on the resulting CF surface can also increase the hydrophilicity of the electrode and improve biofilm formation and development.
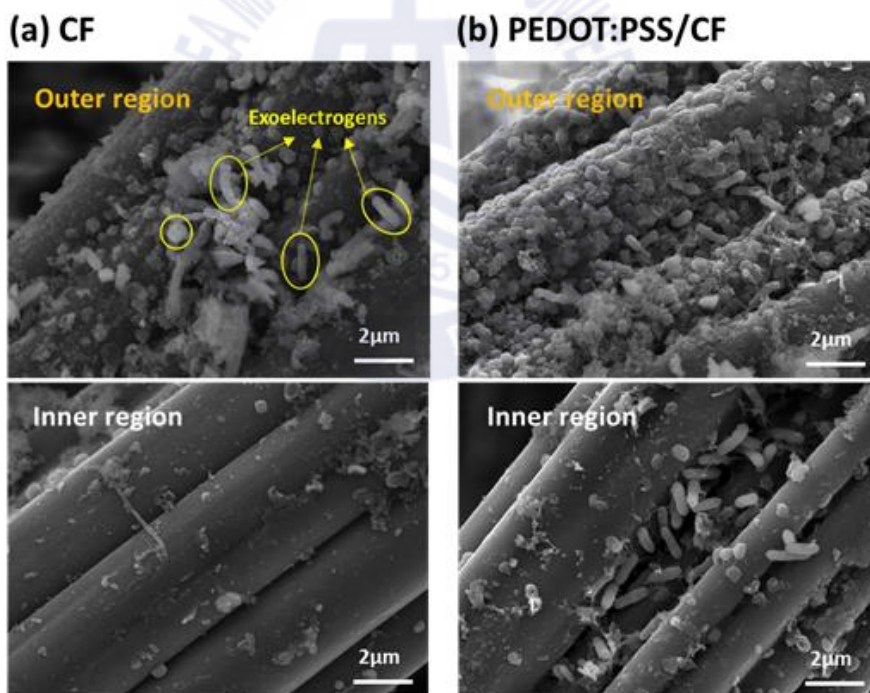
Fig. 3.6. Morphology of bacteria attached to the surface (inner and outer region) of the (a) CF and (b) PEDOT:PSS/CF.

3.3.7 COD removal and columbic efficiency

COD removal and CE percentage of the MECs based on the pristine CF and fabricated PEDOT:PSS/CF shows in Fig. 3.7. COD removal efficiency for both prepared electrodes were 60% higher. COD removal efficiency of PEDOT:PSS/CF (66.3%) was higher than CF (62.9%) as a control, which confirms the higher potential of MEC technology for wastewater treatment. Furthermore, CE calculated based measurement of current and COD removal efficiency, CE of PEDOT:PSS/CF (47.3%) also indicated 1.24-fold greater compared to CF (38.0%).
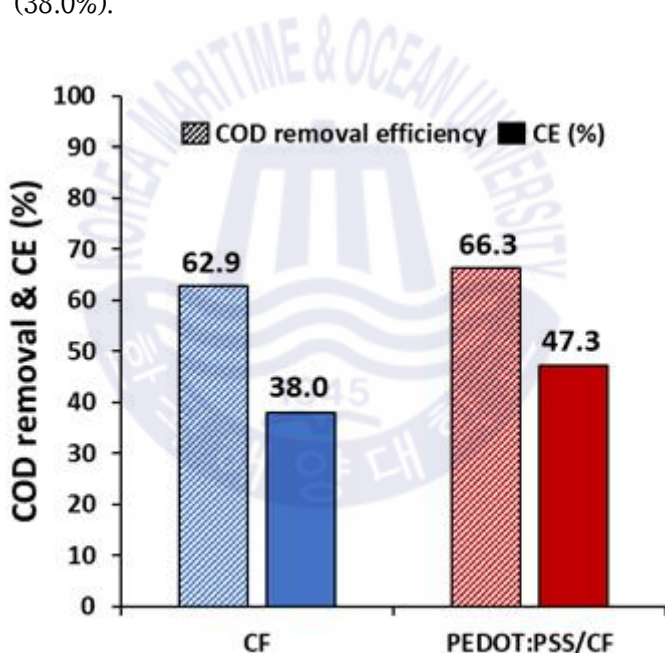
Fig. 3.7. COD removal and columbic efficiency of CF and PEDOT:PSS/CF.

3.4 Conclusions

PEDOT:PSS thin layer was successfully doped to the surface of CF as carbonaceous cathode material by electropolymerization. PEDOT;PSS strongly changed the hydrophobic CF into a super-hydrophilic material. The electropolymerized PEDOT:PSS/CF greatly improved the electrical activity at high charge current density in the neutral state, resulting in very low resistance. The fabricated PEDOT:PSS/CF as an anode in MEC showed that not only the amount of hydrogen generated (33.4% increase) but also the rate (1.65-fold) was improved, and the time of production was also four batches faster than that of CF. This was confirmed by the presence of more microorganisms on the electrode surface of the bio anode after MEC application. In particular, unlike CF, PEDOT:PSS/CF, through the presence of microorganisms up to the inside of the electrode, was able to improve the MEC performance by utilizing the whole area. In addition, PEDOT:PSS/CF showed higher pollutant removal and coulombic efficiency compared to control (CF). Therefore, PEDOT:PSS enhanced MEC performance by converting the entire region of hydrophobic CF into hydrophilicity and improving electroactivity.

3.5 references

[1] Choi M-J, Yang E, Yu H-W, Kim IS, Oh S-E, Chae K-J. Transition metal/carbon nanoparticle composite catalysts as platinum substitutes for bioelectrochemical hydrogen production using microbial electrolysis cells. Int J Hydrogen Energy. 2019;44:2258-65.

[2] Kim K-R, Kang J, Chae K-J. Improvement in methanogenesis by incorporating transition metal nanoparticles and granular activated carbon composites in microbial electrolysis cells. Int J Hydrogen Energy. 2017;42:27623-9.

[3] Yang E, Chae K-J, Choi M-J, He Z, Kim IS. Critical review of bioelectrochemical systems integrated with membrane-based technologies for desalination, energy self-sufficiency, and high-efficiency water and wastewater treatment. Desalination. 2019;452:40-67.

[4] Ajayi FF, Kim K-Y, Chae K-J, Choi M-J, Kim S-Y, Chang I-S, et al. Study of hydrogen production in light assisted microbial electrolysis cell operated with dye sensitized solar cell. Int J Hydrogen Energy. 2009;34:9297-304.

[5] Chae K-J, Choi M-J, Kim K-Y, Ajayi FF, Chang I-S, Kim IS. Selective inhibition of methanogens for the improvement of biohydrogen production in microbial electrolysis cells. Int J Hydrogen Energy. 2010;35:13379-86.

[6] Park S-G, Rhee C, Shin SG, Shin J, Mohamed HO, Choi Y-J, et al. Methanogenesis stimulation and inhibition for the production of different target electrobiofuels in microbial electrolysis cells through an on-demand control strategy using the coenzyme M and 2-bromoethanesulfonate. Environ Int. 2019;131:105006.

[7] Torres C, Krajmalnik-Brown R, Parameswaran P, Marcus A, Wanger G, Gorby Y, et al. Selecting Anode-Respiring Bacteria Based on Anode Potential:

Phylogenetic, Electrochemical, and Microscopic Characterization. Environ Sci Technol. 2009;43:9519-24.

[8] Mohamed HO, Obaid M, Poo K-M, Ali Abdelkareem M, Talas SA, Fadali OA, et al. Fe/Fe2O3 nanoparticles as anode catalyst for exclusive power generation and degradation of organic compounds using microbial fuel cell. Chem Eng J. 2018;349:800-7.

[9] Zhao Y, Dong Z, Wang Y, Li J, An X, Yang D. Process kinetics for the electrocatalytic hydrogen evolution reaction on carbon-based Ni/NiO nanocomposite in a single-chamber microbial electrolysis cell. Int J Hydrogen Energy. 2019;44:28841-7.

[10] Mashkour M, Rahimnejad M. Effect of various carbon-based cathode electrodes on the performance of microbial fuel cell. Biofuel Res J. 2015;2:296-300.

[11] Fan Y, Xu S, Schaller R, Jiao J, Chaplen F, Liu H. Nanoparticle decorated anodes for enhanced current generation in microbial electrochemical cells. Biosens Bioelectron. 2011;26:1908-12.

[12] Kalathil S, Patil S, Pant D. Microbial Fuel Cells: Electrode Materials. 2017.

[13] Erbay C, Yang G, Figueiredo P, Sadr R, Yu C, Han A. Three-dimensional porous carbon nanotube sponges for high-performance anodes of microbial fuel cells. J Power Sources. 2015;298:177-83.

[14] Han TH, Sawant SY, Hwang S-J, Cho MH. Three-dimensional, highly porous N-doped carbon foam as microorganism propitious, efficient anode for high performance microbial fuel cell. RSC Advances. 2016;6:25799-807.

[15] Koo H, Allan RN, Howlin RP, Stoodley P, Hall-Stoodley L. Targeting microbial biofilms: current and prospective therapeutic strategies. Nature reviews Microbiology. 2017;15:740-55.

[16] Pareek A, Sravan JS, Mohan SV. Fabrication of three-dimensional graphene anode for augmenting performance in microbial fuel cells. Carbon Resources Conversion. 2019.

[17] Cai T, Huang M, Huang Y, Zheng W. Enhanced performance of microbial fuel cells by electrospinning carbon nanofibers hybrid carbon nanotubes composite anode. Int J Hydrogen Energy. 2019;44:3088-98.

[18] Yu Y-Y, Zhai D-D, Si R-W, Sun J-Z, Liu X, Yong Y-C. Three-Dimensional Electrodes for High-Performance Bioelectrochemical Systems. Int J Mol Sci. 2017;18:90.

[19] Zhang Y, Liu L, Van der Bruggen B, Yang F. Nanocarbon based composite electrodes and their application in microbial fuel cells. Journal of Materials Chemistry A. 2017;5:12673-98.

[20] Hou J, Liu Z, Zhang P. A new method for fabrication of graphene/polyaniline nanocomplex modified microbial fuel cell anodes. J Power Sources. 2013;224:139-44.

[21] Cui H-F, Du L, Guo P-B, Zhu B, Luong JHT. Controlled modification of carbon nanotubes and polyaniline on macroporous graphite felt for high-performance microbial fuel cell anode. J Power Sources. 2015;283:46-53.

[22] Li F, Wang D, Liu Q, Wang B, Zhong W, Li M, et al. The construction of rod-like polypyrrole network on hard magnetic porous textile anodes for microbial fuel cells with ultra-high output power density. J Power Sources. 2019;412:514-9.

[23] Mantione D, Del Agua I, Sanchez-Sanchez A, Mecerreyes D. Poly (3, 4-ethylenedioxythiophene)(PEDOT) derivatives: innovative conductive polymers for bioelectronics. Polymers. 2017;9:354.

[24] Chiolerio A, Rivolo P, Porro S, Stassi S, Ricciardi S, Mandracci P, et al.

Inkjet-printed PEDOT: PSS electrodes on plasma-modified PDMS nanocomposites: Quantifying plasma treatment hardness. Rsc Advances. 2014;4:51477-85.

[25] Aryal N, Tremblay P-L, Xu M, Daugaard AE, Zhang T. Highly conductive poly (3, 4-ethylenedioxythiophene) polystyrene sulfonate polymer coated cathode for the microbial electrosynthesis of acetate from carbon dioxide. Frontiers in Energy Research. 2018;6:72.

[26] Luo J, Billep D, Waechtler T, Otto T, Toader M, Gordan O, et al. Enhancement of the thermoelectric properties of PEDOT:PSS thin films by post-treatment. Journal of Materials Chemistry A. 2013;1:7576-83.

[27] Duc C, Vlandas A, Malliaras GG, Senez V. Wettability of PEDOT:PSS films. Soft Matter. 2016;12:5146-53.

[28] Alemu D, Wei H-Y, Ho K-C, Chu C-W. Highly conductive PEDOT: PSS electrode by simple film treatment with methanol for ITO-free polymer solar cells. Energy Environ Sci. 2012;5:9662-71.

[29] Kang YL, Ibrahim S, Saravanan P. Synergetic effect of conductive polymer poly(3,4-ethylenedioxythiophene) with different structural configuration of anode for microbial fuel cell application. Bioresour Technol. 2015;189:364-9.

[30] Zajdel TJ, Baruch M, Méhes G, Stavrinidou E, Berggren M, Maharbiz MM, et al. PEDOT:PSS-based Multilayer Bacterial-Composite Films for Bioelectronics. Scientific Reports. 2018;8:15293.

[31] Chang SH, Chiang C, Kao F, Tien C, Wu C. Unraveling the Enhanced Electrical Conductivity of PEDOT:PSS Thin Films for ITO-Free Organic Photovoltaics. IEEE Photonics Journal. 2014;6:1-7.

[32] Xiong S, Zhang L, Lu X. Conductivities enhancement of poly (3, 4-ethylenedioxythiophene)/poly (styrene sulfonate) transparent electrodes with

diol additives. Polym Bull. 2013;70:237–47.

[33] Lindfors T, Boeva ZA, Latonen R-M. Electrochemical synthesis of poly (3, 4-ethylenedioxythiophene) in aqueous dispersion of high porosity reduced graphene oxide. RSC Advances. 2014;4:25279–86.

[34] Kim SH, Kim JH, Choi HJ, Park J. Pickering emulsion polymerized poly (3, 4-ethylenedioxythiophene): poly (styrenesulfonate)/polystyrene composite particles and their electric stimuli-response. RSC Advances. 2015;5:72387–93.

[35] Funda S, Ohki T, Liu Q, Hossain J, Ishimaru Y, Ueno K, et al. Correlation between the fine structure of spin-coated PEDOT: PSS and the photovoltaic performance of organic/crystalline-silicon heterojunction solar cells. J Appl Phys. 2016;120:033103.

[36] Xu S, Liu C, Xiao Z, Zhong W, Luo Y, Ou H, et al. Cooperative effect of carbon black and dimethyl sulfoxide on PEDOT: PSS hole transport layer for inverted planar perovskite solar cells. Solar Energy. 2017;157:125–32.

[37] Han Y-K, Chang M-Y, Li H-Y, Ho K-S, Hsieh T-H, Huang P-C. In situ synthesis and deposition of conducting PEDOT:PSS nanospheres on ITO-free flexible substrates. Mater Lett. 2014;117:146–9.

[38] Susanti E, Wulandari P. Effect of localized surface plasmon resonance from incorporated gold nanoparticles in PEDOT: PSS hole transport layer for hybrid solar cell applications. Journal of Physics: Conference Series: IOP Publishing; 2018. p. 012010.

[39] Xu S, Liu C, Xiao Z, Zhong W, Luo Y, Ou H, et al. Cooperative effect of carbon black and dimethyl sulfoxide on PEDOT:PSS hole transport layer for inverted planar perovskite solar cells. Solar Energy. 2017;157:125–32.

[40] Olivares AJ, Cosme I, Sanchez-Vergara ME, Mansurova S, Carrillo JC, Martinez HE, et al. Nanostructural Modification of PEDOT: PSS for High

Charge Carrier Collection in Hybrid Frontal Interface of Solar Cells. Polymers. 2019;11:1034.

[41] Chu CW, Mengistie DA, Wang P-C. Effect of Molecular Weight of Additives on the Conductivity of PEDOT:PSS and Efficiency for ITO-free Organic Solar Cells. J Mater Chem A. 2013;1.

[42] Li F, An X, Wu D, Xu J, Chen Y, Li W, et al. Engineering Microbial Consortia for High-Performance Cellulosic Hydrolyzates-Fed Microbial Fuel Cells. Frontiers in microbiology. 2019;10:409.

Chapter 4. Conclusion

As a bioelectrochemical cell technology, the electrodes of MFC and MEC materials has been modified cost-effectively to improve the performance.

In the case of MFC, the cathode of carbon-based materials using nickel nanoparticles as a non-platinum catalyst was modified to improve the air-cathode MFC performance. The uniform deposition of nickel particles and the presence of nickel oxides contributed to electrical conductivity and improvement of ORR, resulting in a power density 4-times higher than commercial Pt/C. In MEC, the performance of MEC for hydrogen production was improved by doping PEDOT:PSS, a conductive polymer, on a three-dimensional porous carbon felt and reforming the anode. PEDOT:PSS with thin layers improves electrical conductivity and hydrophilicity, allowing microorganisms to be well deposited in all regions of the electrode, improving hydrogen production (33.4%) and control ratio (1.65 times).

Overall, it is important to develop catalysts and modifiers according to the characteristics of electrodes to improve the performance of biochemical batteries and to develop a method to improve the catalytic performance.

Academic achievement

Peer-reviewed journal article (International)

1. Son E-B, Poo K-M, Mohamed HO, **Choi Y-J,** Cho W-C, Chae K-J. A novel approach to developing a reusable marine macro-algae adsorbent with chitosan and ferric oxide for simultaneous efficient heavy metal removal and easy magnetic separation. Bioresour Technol. 2018;259:381-7.

2. Poo K-M, Son E-B, Chang J-S, Ren X, **Choi Y-J,** Chae K-J. Biochars derived from wasted marine macro-algae (Saccharina japonica and Sargassum fusiforme) and their potential for heavy metal removal in aqueous solution. J Environ Manag. 2018;206:364-72.

3. Mohamed HO, Sayed ET, Obaid M, **Choi Y-J,** Park S-G, Al-Qaradawi S, Chae K-J. Transition metal nanoparticles doped carbon paper as a cost-effective anode in a microbial fuel cell powered by pure and mixed biocatalyst cultures. Int J Hydrogen Energy. 2018;43:21560-71.

4. Park S-G, Rhee C, Shin SG, Shin J, Mohamed HO, **Choi Y-J,** Chae K-J. Methanogenesis stimulation and inhibition for the production of different target electrobiofuels in microbial electrolysis cells through an on-demand control strategy using the coenzyme M and 2-bromoethanesulfonate. Environ Int. 2019;131:105006.

5. **Choi Y-J,** Mohamed HO, Park S-G, Al Mayyahi RB, Al-Dhaifallah M, Rezk H, Ren X, Yu H, Chae K-J. Electrophoretically fabricated nickel/nickel oxides as cost effective nanocatalysts for the oxygen reduction reaction in air-cathode microbial fuel cell. Int J Hydrogen Energy. 2019.

6. Eisa T, Mohamed HO, **Choi Y-J,** Park S-G, Al Rafeeah, Al Abdelkareem M, Oh S-E, Chae K-J. Nickel Nanorods over Nickel Foam as Standalone Anode for Direct Alkaline Methanol and Ethanol Fuel Cell. Int J Hydrogen Energy. 2019.

Conference presentations (International)

1. **Choi Y-J**, Son E-B, Poo K-M, Chae K-J, "Influence of Pyrolysis Temperature on Hijikia Biochar Property and Function as a Heavy metal (Cd, Cu, Zn) Sorbent in Aqueous Solution", The 2nd International Conference on Biological Waste as Resource (BWR), Polytechnic university, Hong Kong, May, 25-28, 2017. Postar presentation.

7. Son E-B, **Choi Y-J**, Poo K-M, Chang J-S, Chae K-J, "Heavy metal removal from aqueous solution using engineered-magnetic biochars derived from waste algal biomass.", The 2nd International Conference on Biological Waste as Resource (BWR), Polytechnic university, Hong Kong, May, 25-28, 2017. Oral presentation.

8. **Choi Y-J**, Mohamed HO, Park S-G, Chae K-J, "Evaluation of varies metal catalyst (Ni, Cd and Co) doped cathode to alternative Pt for Microbial Fuel cells (MFCs)", The 2nd International conference on Bioresources, Energy, Environment, and Materials technology (BEEM), Vivaldi park, Hongcheon, Korea, Jun, 10-13, 2018. Oral presentation.

9. Park S-G, **Choi Y-J**, Kim T-N, Mohamed Hend, Shin S-G, Chae K-J, "Investigating the effect of bio-stimulation and inhibition on biogas production in microbial electrolysis cell.", The 2nd International conference on Bioresources, Energy, Environment, and Materials technology (BEEM), Vivaldi park, Hongcheon, Korea, Jun, 10-13, 2018. Oral presentation.

10. Park S-G, Lee J-E, Mohamed HO, **Choi Y-J**, Chae K-J, "Development of anti-biofouling proton exchange membrane incorporating silver nanoparticles and polydopamine for sustainable operation of microbial electrolysis cells.", The 3rd International Conference on Alternative Fuels, Energy and Environment (ICAFEE), Nanjing, LiuYuan Hotel, October, 30, 2018. Oral presentation.

11. Lee J-E, **Choi Y-J**, Kim T-N, Park G-Y, Gong Y-K, Koo S-R, Seo J-P, Jeong J-W, Kim S-Y, Chae K-J, "Examination of physico-chemical properties of microplastics in wastewater", The 7th Busan Global Water Forum, Bexco, Busan, September, 18-19, 2019, Poster presentation.

12. Cho W-C, Lee J-E, Poo K-M, **Choi Y-J,** Son E-B, Chae K-J, "Advanced electrochemical oxidation and biochar adsorbent for VOCs removal from oily hazardous wastewater", The 7th Busan Global Water Forum, Bexco, Busan, September, 18-19, 2019, Poster presentation.

13. **Choi Y-J**, Park S-G, Rajesh P. P, Chae K-J, "Highly hydrophilic, conductive, biocompatible 3D porous electrode fabrication using multifunctional PEDOT:PSS polymer for electrohydrogenesis in microbial electrolysis cell", December, 10-13, 2019, Oral presentation.

Conference presentations (Domestic)

1. 손은비, **최윤정**, 김경록, 부경민, 채규정, "다양한 열분해 온도에서 제조된 다시마와 톳 바이오차의 물리적 특성 및 수중 중금속 (Cd, Cu, Zn) 제거능 평가", 한국물환경학회, 김대중컨벤션센터, 광주, 대한민국, 3월, 23-24, 2017.

2. 부경민, 김태남, **최윤정**, 김인수, 김곤, 채규정, "Development of a system to prevent harmful chemical substances from leaking out of water through pipeline at the time of occurrence of chemical accident in industrial complex", Korea Society of Environmental Engineers, 대한환경공학회, ICC 제주, 대한민국, 11월, 15-17, 2017.

3. **최윤정,** Mohamed, H.O., Mayyahi, R.B. Al., 박성관, 채규정, "전기영동증착 기술을 이용한 미생물연료전지의 비백금 Ni/NiO_x 나노촉매의 합성", 2018 대한환경공학회, 광주, 대한민국, 11월, 14-16, 2018.

4. 박성관, 이채영, 신승구, 신주희, Mohamed, H.O., **최윤정,** 채규정, "생물전기연료 생산을 위한 메탄균의 활성 촉진과 억제 전략 및 미생물전해전지 내 미생물 군집 특성 연구", 2018 대한환경공학회, 광주, 대한민국, 11월, 14-16, 2018.

5. **최윤정**, 정지현, 박상호, 신혁선, 김상준, 김동환, 채규정, "온도, SS 및 염도별 조건과 측정 기기에 따른 해수에서의 총잔류염소 정량화를 위한 비교 평가", 2019 대한환경공학회, 부산, 대한민국, 12월, 10-13, 2019.

Patent

1. Chae K-J, Chang J-S, Poo K-M, Son E-B, **Choi Y-J**, Manufacturing method of Biochar for removing heavy metal and biochar manufactured therefrom and absorbent comprising of the biochar for removing heavy metal, 10-2017-0017017, Application, 2017, Republic of Korea.

감사의 글

어느덧 2년 동안의 석사과정이 지나고 졸업논문이 나오기까지 수많은 사람의 도움을 받았습니다. 그분들의 도움이 없었다면 이 논문이 나올 수 없었을 것이기에 이 자리를 빌려 감사의 인사를 드리고자 합니다.

가장 먼저 부족한 저를 끝까지 이끌어주시고 지도해주신 채규정 교수님께 감사드립니다. 연구에 대해 아무것도 모르던 저에게 성심성의껏 알려주시고 인생에 필요한 지혜를 가르쳐주셨습니다. 감사합니다. 또한, 매 수업 시간마다 열정적으로 가르쳐주신 송영채 교수님, 바이오차 실험 때 많은 조언을 해주신 장재수 교수님, 졸업논문발표 때 날카로운 지적과 따뜻한 조언을 해주신 고성철 교수님, 김명진 교수님, 유근제 교수님께 큰 감사를 표합니다.

같은 길을 함께 걸어온 WENL 연구실 사람들, 그들이 있었기에 행복했습니다. 모든 게 서툰 저에게 힘든 기색 없이 잘 알려주었고 실수가 있어도 넓은 마음으로 이해해주었던 랩매니저 성관이 오빠, 동기로써 많은 시간을 함께하고 의지했으며 강한 통찰력으로 더 성장할 수 있게 도와준 태남이 오빠, 학부 동안 귀찮을 정도로 물어봐도 잘 가르쳐준 경록이 오빠, 재밌는 이야기로 즐거운 연구실 생활을 할 수 있게 만들어준 완철이 오빠, 항상 옆에서 사소한 것까지 하나하나 챙겨준 꼼꼼한 은비 언니, 선배로서 못 해준 게 많아 미안한 세림, 가영, 전기화학 신인 Tasnim으로부터 정말 많이 배웠습니다. 짧은 시간이었지만 영어 교정을 도와준 Riyam, Rajesh 박사님, 제 연구의 대부분을 함께해주신 Hend 박사님께 정말 감사드립니다. 못하는 실험이 없도록 무엇이든 만들어주신 최철림 대표님, 그리고 다른 분야를 연구했지만 내 일처럼 도와주시고 가르쳐주신 부경민 박사님, 이지은 박사님께 감사의 말씀을 전합니다.

다른 실험실이지만 도와주시고 함께해주신 동기와 선배님들이 있었기에 연구에 더욱 전념할 수 있었습니다. 바쁜 와중에도 선뜻 도와준 경근이 오빠, 태선이 오빠, 한초 오빠, 풍경 교수님 정말 감사합니다. 늘 친동생처럼 챙겨준 채영이 언니, 준혁이 오빠, 정신적 버팀목이 되어준 지현이, 해양대에서 가장 많은 시간을 함께한 희소, 인생 상담사 혜림, 너무나도 착한 선미, 맨날 실수해서 힘들었을 텐데 괜찮다고 말해주는 조교 선생님 은진이, 정말 고맙습니다.

　　이 외에도 저를 스쳐 간 모든 분께 감사의 말씀을 전합니다.

　　마지막으로 언제나 변함없이 딸을 믿고 지원해주시는 아버지 어머니께 감사의 인사를 드립니다. 아낌없는 성원을 보내주신 그들이 있었기에 힘든 상황에도 굴하지 않고 이겨낼 수 있었습니다. 사랑합니다.

　　이렇게 많은 분들의 도움이 있었기에 무사히 졸업을 하게 되었습니다. 이러한 도움이 더욱 빛나도록 앞으로도 최선을 다하겠습니다. 감사합니다.

2020년 1월

최윤정 올림.